JOURNAL OF PROPULSION AND POWER
Vol. 19, No. 5, September–October 2003

Acoustic Analysis of Gas Turbine Combustors

Ann P. Dowling* and Simon R. Stow†
University of Cambridge, Cambridge, England CB2 1PZ, United Kingdom

Combustion instability has become a major issue for gas turbine manufacturers. Stricter emission regulations, particularly on nitrogen oxides, have led to the development of new combustion methods, such as lean premixed prevaporized (LPP) combustion, to replace the traditional diffusion flame. However, LPP combustion is much more liable to generate strong oscillations, which can damage equipment and limit operating conditions. As a tutorial, methods to investigate combustion instabilities are reviewed. The emphasis is on gas turbine applications and LPP combustion. The flow is modeled as a one-dimensional mean with linear perturbations. Calculations are typically done in the frequency domain. The techniques described lead to predictions for the frequencies of oscillations and the susceptibility to instabilities for which linear disturbances grow expotentially in time. Appropriate boundary conditions are discussed, as is the change in the linearized flow across zones of heat addition and/or area change. Many of the key concepts are first introduced by considering one-dimensional perturbations. Later higher-order modes, particularly circumferential waves, are introduced, and modal coupling is discussed. The modeling of a simplified combustion system, from compressor outlet to turbine inlet, is described. The approaches are simple and fast enough to be used at the design stage.

Introduction

LEAN premixed prevaporized (LPP) gas turbine combustors have the great advantage of very low NOx emission. However, they are susceptible to instability. These instabilities involve coupling between the rate of combustion and acoustic waves in the combustor: Essentially unsteady combustion generates acoustic waves, which alter the inlet flow rates of fuel and air. At lean premixed conditions, this changed fuel–air ratio leads to significant unsteady combustion. If the phase relationship is suitable,[1] self-excited oscillations grow. Because acoustic waves play such a central role in this phenomenon, the frequencies of the combustion oscillations tend to be close to the acoustic resonance frequencies of the combustion system. Although the coupling between the combustion and the acoustics modifies the frequencies of oscillation, under many circumstances the shift in frequency is small. A complete analysis of this phenomenon requires the capability to model and understand the acoustic modes of the combustion system and to couple these to a flame model that describes the unsteady combustion response to these acoustic disturbances. Although the drive for low emissions has made gas turbine combustors particularly susceptible to instability, such oscillations have long been an issue for other combustion systems, for example, rocket motors.[2,3]

This paper is structured as a tutorial. It starts with the equations of motion and investigates the form of linear disturbances. In a region of uniform mean flow, these are found to consist of acoustic, vortical, and entropic disturbances. We begin by investigating one-dimensional disturbances, in which these linearized waves are functions of a single spatial variable and time, propagating in a duct of uniform cross-sectional area. After application of appropriate boundary conditions, the mode shape and resonant frequencies are determined. The analysis is gradually developed, adding incrementally various effects that characterize gas turbine combustors. These include unsteady heat addition, mean temperature gradients, and a mean flow velocity. We investigate how these effects alter the frequencies of oscillation and the mode shapes. In this paper, we concentrate on an acoustic analysis of gas turbine combustors. The discussion of flame models is in a companion paper in this issue,[4] and here we consider the dependence unsteady heat release on fuel–air ratio, which is widely recognized as the major cause of instability in LPP combustors. However, the techniques described could be used with any flame model for other configurations.

The one-dimensional examples introduce many of the key concepts, but need extension to be applicable to annular combustors, in which the longest combustor dimension can be its circumference. This means the lowest resonance frequency is associated with modes that propagate in the azimuthal direction. We, therefore, extend the modal analysis to annular and cylindrical geometries. Then the axial phase speed of acoustic waves is usually a function of frequency and some modes are cutoff, decaying exponentially with axial distance.

In an LPP combustor, the acoustics from compressor exit to turbine entry can influence the combustion instabilities. We note how this combustion system can be represented by a series of annular and cylindrical ducts and describe how these ducts can be joined to determine the resonance frequencies of the complex system.[5–10] Finally, we note that, when the geometry is no longer axisymmetric, modal coupling may occur and describe the influence of that on the frequencies of instability and the modeshape.

Linearized Equations of Motion

Because this paper aims to be an introductory tutorial, we will start from the full equations of motion and derive their linearized form. For a compressible viscous fluid in the absence of external forces, conservation of mass and momentum lead to the Navier–Stokes equations,

$$\frac{\mathrm{D}\rho}{\mathrm{D}t} + \rho\nabla\cdot\boldsymbol{u} = 0 \tag{1a}$$

$$\rho\frac{\mathrm{D}\boldsymbol{u}}{\mathrm{D}t} = -\nabla p + \frac{\partial\sigma_{i,j}}{\partial x_j}\boldsymbol{e}_i \tag{1b}$$

where p is the pressure, ρ is the density, $\boldsymbol{u}$ is the velocity, and $\sigma_{i,j}$ is the viscous stress tensor. Here $\mathrm{D}/\mathrm{D}t$ is the material derivative, $\partial/\partial t + \boldsymbol{u}\cdot\nabla$, and $\boldsymbol{e}_i$ represents the unit vector in the direction of coordinate i. For a perfect gas, we have the gas law $p = R_{\mathrm{gas}}\rho T$, where T is the temperature, $R_{\mathrm{gas}} = c_p - c_v$ is the gas constant, and c_p and c_v are the specific heats at constant pressure and volume, respectively. The internal energy per unit mass, e, is equal to $c_v T$, and the enthalpy h is $c_p T = e + p/\rho$. Conservation of energy gives

Received 8 May 2003; revision received 30 June 2003; accepted for publication 30 June 2003.

*Professor of Mechanical Engineering, Department of Engineering. Senior Member AIAA.
†Research Associate, Department of Engineering.

the energy equation,

$$\rho\frac{\mathrm{D}}{\mathrm{D}t}\left(e+\frac{1}{2}\boldsymbol{u}^2\right)=-\boldsymbol{\nabla}\cdot(p\boldsymbol{u})+q+\boldsymbol{\nabla}\cdot(k\boldsymbol{\nabla}T)+\frac{\partial}{\partial x_j}(\sigma_{i,j}u_i) \tag{2}$$

where k is the conductivity and q is the rate of heat added to the fluid per unit volume. When Eq. (1b) is used, this can be written as

$$\rho\frac{\mathrm{D}h}{\mathrm{D}t}=\frac{\mathrm{D}p}{\mathrm{D}t}+q+\boldsymbol{\nabla}\cdot(k\boldsymbol{\nabla}T)+\sigma_{i,j}\frac{\partial u_i}{\partial x_j} \tag{3}$$

We define entropy S by the thermodynamic relation $\mathrm{d}h=T\,\mathrm{d}S+(1/\rho)\mathrm{d}p$. Hence, Eq. (3) gives that

$$\rho T\frac{\mathrm{D}S}{\mathrm{D}t}=q+\boldsymbol{\nabla}\cdot(k\boldsymbol{\nabla}T)+\sigma_{i,j}\frac{\partial u_i}{\partial x_j} \tag{4}$$

showing that it is heat input, heat transfer, and viscous effects that lead to an entropy increase for a material particle. Taking the curl of Eq. (1b) and using Eq. (1a) gives an equation for the development of the vorticity, $\boldsymbol{\xi}=\boldsymbol{\nabla}\times\boldsymbol{u}$,

$$\frac{\mathrm{D}}{\mathrm{D}t}\left(\frac{\boldsymbol{\xi}}{\rho}\right)=\left(\frac{\boldsymbol{\xi}}{\rho}\cdot\boldsymbol{\nabla}\right)\boldsymbol{u}+\frac{1}{\rho^3}\boldsymbol{\nabla}\rho\times\boldsymbol{\nabla}p+\frac{1}{\rho}\boldsymbol{\nabla}\times\left(\frac{1}{\rho}\frac{\partial\sigma_{i,j}}{\partial x_j}\boldsymbol{e}_i\right) \tag{5}$$

The first term on the right-hand side describes how the stretching of vortex lines intensifies the local vorticity, and clearly the last term represents generation of vorticity by viscous effects. The second term shows that vorticity can be created when the pressure gradient and density gradient are not aligned. An example of this would be an acoustic pressure oscillation with a component normal to a flame front (density gradient), so that, for instance, circumferential waves will generate vorticity at combustion zones.

We will now assume inviscid flow ($\sigma_{i,j}\equiv 0$). We will also assume the fluid is an ideal gas, that is, in addition to being a perfect gas there is no heat conduction, and we take c_p and c_v to be constant. From the preceding definition of entropy, we find that $S=c_v\log(p/\rho^\gamma)$ (plus an arbitrary constant, which we set to zero), where $\gamma=c_p/c_v$ is the ratio of specific heats. We take the flow to be composed of a steady uniform mean flow (denoted by overbars) and a small perturbation (denoted by primes),

$$p(\boldsymbol{x},t)=\bar{p}+p'(\boldsymbol{x},t) \tag{6}$$

and similarly for the other flow variables. (Note that the overbars denote the time mean of all variables, not the density-weighted Favre averages that would be more common in combustion.) From Eqs. (1), (4), and (5), the linearized equations for these perturbations are

$$\frac{\bar{\mathrm{D}}\rho'}{\mathrm{D}t}+\bar{\rho}\boldsymbol{\nabla}\cdot\boldsymbol{u}'=0 \tag{7a}$$

$$\frac{\bar{\mathrm{D}}\boldsymbol{u}'}{\mathrm{D}t}+\frac{1}{\bar{\rho}}\boldsymbol{\nabla}p'=\boldsymbol{0} \tag{7b}$$

$$\bar{\rho}\bar{T}\frac{\bar{\mathrm{D}}S'}{\mathrm{D}t}=q' \tag{7c}$$

$$\frac{\mathrm{D}\boldsymbol{\xi}'}{\mathrm{D}t}=\boldsymbol{0} \tag{7d}$$

where $\bar{\mathrm{D}}/\mathrm{D}t=\partial/\partial t+\bar{u}\cdot\boldsymbol{\nabla}$ and we have used that $\bar{\boldsymbol{\xi}}=\boldsymbol{0}$. Combining Eqs. (7a–7c) and using $S'=c_v p'/\bar{p}-c_p\rho'/\bar{\rho}=0$ leads to the inhomogeneous wave equation,

$$\frac{1}{\bar{c}^2}\frac{\bar{\mathrm{D}}^2p'}{\mathrm{D}t^2}-\nabla^2p'=\frac{\gamma-1}{\bar{c}^2}\frac{\bar{\mathrm{D}}q'}{\mathrm{D}t} \tag{8}$$

where c is the speed of sound. We see that the vorticity equation (7d) is not coupled to either the pressure or the entropy. For no unsteady heat input, the pressure equation (8) and entropy equation (7c) are also uncoupled. Any perturbation can then be thought of as the sum of three types of disturbance,[11] 1) an acoustic disturbance that is isentropic and irrotational, 2) an entropy disturbance that is incompressible and irrotational, and 3) a vorticity disturbance that is incompressible and isentropic. These three types are independent and can be considered separately. For the pressure (acoustic) disturbance, we have $S'=0$ and $\boldsymbol{\xi}'=\boldsymbol{0}$; hence $\rho'=p'/\bar{c}^2$. Because $q'=0$, Eq. (8) becomes the convected wave equation for p',

$$\left(\frac{1}{\bar{c}^2}\frac{\bar{\mathrm{D}}^2}{\mathrm{D}t^2}-\nabla^2\right)p'=0 \tag{9}$$

with the corresponding u' being given by Eq. (7b). These solutions are acoustic waves; relative to the fluid, these propagate at the speed of sound in all directions. For the entropic disturbance, $p'=0$ and $\boldsymbol{u}'=\boldsymbol{0}$. From Eq. (7c), we see that the entropy wave is stationary relative to the fluid, that is, it is convected with the mean flow; this is sometimes referred to as a convected hot spot. For the vortical disturbance, $p'=\rho'=0$ and $\boldsymbol{\nabla}\cdot\boldsymbol{u}'=\boldsymbol{0}$, and Eq. (7d) shows that this is also convected with the mean flow. If the mean flow is zero, only acoustic disturbances propagate.

Conditions Across a Flame Zone

We now consider the affect of a thin flame zone in the plane $x=0$, where we take the rate of heat input per unit area to be Q_A. There will be a discontinuity in the flow parameters across the flame; we denote conditions at $x=0_-$ and $x=0_+$ by subscripts 1 and 2, respectively. From Eqs. (1) and (3), we find that

$$\rho_2u_2=\rho_1u_1 \tag{10a}$$

$$p_2+\rho_2u_2^2=p_1+\rho_1u_1^2 \tag{10b}$$

$$\rho_2u_2H_2=\rho_1u_1H_1+Q_A \tag{10c}$$

where $H=h+\frac{1}{2}u^2$ is the stagnation enthalpy. To calculate the mean flow, we assume that $\bar{Q}_A$ is known (from knowledge of the fuel type, equivalence ratio, etc.). A flame model is used to describe the dependence of Q'_A on the flow perturbations (see Lieuwen[4]).

Boundary Conditions

At the inlet and outlet of the combustion system, there are boundary conditions that the perturbations must satisfy. If the outlet discharges into the atmosphere or a large plenum chamber (as is often the case for combustor test rigs) we may model this as a open end, taking $p'(r,\theta,t)=0$. If the inlet is supplied by a plenum chamber we may treat this also as an open end [$p'(r,\theta,t)=0$] and additionally assume that there are no entropy or vorticity disturbances present. The compressor exit and turbine inlet of a gas turbine can be modeled as a choked inlet and choked outlet, respectively, to the combustion system. Marble and Candel[12] showed that for one-dimensional perturbations the boundary condition of constant nondimensional mass flow rate at a compact choked outlet reduces to

$$2(u'/\bar{u})+\rho'/\bar{\rho}-p'/\bar{p}=0 \tag{11}$$

Stow et al.[13] have shown that this condition still applies for circumferential-varying disturbances in a narrow annular gap. (Disturbances in narrow annular gap geometries are discussed later.)

For a compact choked inlet, Stow et al.[13] considered the interaction of the shock position and the flow perturbations, finding that for one-dimensional disturbances the perturbations in mass flux and energy flux are zero just after the shock and that for circumferential-varying disturbances in a narrow annular gap the angular-velocity perturbation is also zero. From conservation of mass, energy, and angular momentum, these quantities are also zero at the start of a straight duct with a low Mach number mean flow $\bar{M}_1$ just downstream of the choking plane. This gives the inlet boundary conditions

$$\rho'/\bar{\rho}+u'/\bar{u}=p'/\bar{p}-\rho'/\bar{\rho}+(\gamma-1)\bar{M}_1(u'/\bar{u})=w'=0 \tag{12}$$

For a weak shock, one would expect that there is negligible entropy production. However, the equations imply that the (usually ignored) entropy perturbation downstream of the inlet is in fact comparable to the acoustic oscillations. (In a frame of reference moving with the shock the acoustic perturbations are indeed much larger than the entropy disturbance, but viewed in a stationary frame close to the shock the discrepancy is not as great. After an area increase to a low Mach number region, the acoustic perturbations are smaller still and are then of the same order as the entropy perturbations.) For circumferentially-varying disturbances, a significant vorticity perturbation is also produced.

Other analytical inlet and outlet boundary conditions, such as acoustically closed ends ($u' = 0$) or semi-infinite (nonreflecting) pipes, can also be used. Alternatively, the acoustic impedance of the inlet or outlet can be measuring experimentally using microphones and acoustic source driven over a range of frequencies. (This approach is similar to the measurement of the transfer matrix for a premixer discussed subsequently.)

One-Dimensional Disturbances

Plane Wave Solutions

As an introductory example, let us consider first a duct, with uniform cross-sectional area, mean temperature, and density with no mean flow, in which the unsteady flow parameters are just functions of the axial space coordinate x and time, t. Then the general solution of the wave equation (9) can be written in the form

$$p'(x,t) = f(t - x/\bar{c}) + g(t + x/\bar{c}) \tag{13}$$

where the functions $f(t)$ and $g(t)$ are arbitrary. From the one-dimensional form of the linearized momentum equation (7b), the particle velocity in the x direction is given by

$$\frac{\partial u'}{\partial t} = -\frac{1}{\bar{\rho}}\frac{\partial p'}{\partial x} = \frac{1}{\bar{\rho}\bar{c}}\frac{\partial}{\partial t} f\left(t - \frac{x}{\bar{c}}\right) - \frac{1}{\bar{\rho}\bar{c}}\frac{\partial}{\partial t} g\left(t + \frac{x}{\bar{c}}\right) \tag{14a}$$

that is,

$$u'(x,t) = (1/\bar{\rho}\bar{c})[f(t - x/\bar{c}) - g(t + x/\bar{c})] \tag{14b}$$

For perturbations of frequency ω, it is convenient to write $f(t) = \mathrm{Re}[\hat{f}\exp(i\omega t)]$, where the circumflex denotes a complex amplitude. With this notation,

$$\hat{p}(x) = \hat{f}\exp(-i\omega x/\bar{c}) + \hat{g}\exp(i\omega x/\bar{c}) \tag{15a}$$

$$\hat{u}(x) = (1/\bar{\rho}\bar{c})[\hat{f}\exp(-i\omega x/\bar{c}) - \hat{g}\exp(i\omega x/\bar{c})] \tag{15b}$$

The resonant frequencies follow from application of appropriate boundary conditions at the ends of the duct. For example, with a large plenum attached to the duct end at $x = 0$ and a restriction at $x = l$ as shown in Fig. 1, the appropriate boundary conditions are

$$\hat{p}(0) = \hat{u}(l) = 0 \tag{16}$$

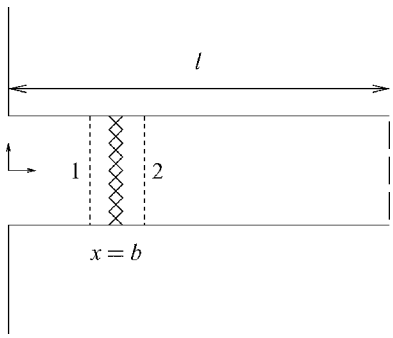

Fig. 1 Boundary conditions in the model problem.

Equation (15a) then leads to $\hat{g} = -\hat{f}$, and it follows directly from Eq. (15b) that

$$\cos(\omega l/\bar{c}) = 0 \tag{17a}$$

with solutions

$$\omega = \omega_n = \left(n - \tfrac{1}{2}\right)(\pi\bar{c}/l) \tag{17b}$$

for integer $n \geq 1$. These are the resonant frequencies ω_n of the duct, describing the oscillations in which the pressure oscillates without decay. The corresponding modeshapes are

$$\hat{p}(x) = A_n \sin[(2n-1)\pi x/2l] \tag{18a}$$

$$\hat{u}(x) = (iA_n/\bar{\rho}\bar{c})\cos[(2n-1)\pi x/2l] \tag{18b}$$

for an arbitrary constant A_n.

With Unsteady Heat Addition

With heat addition at a rate $q(x,t)$/unit volume, the pressure perturbations satisfy an inhomogeneous one-dimensional wave equation that follows from setting $\bar{u} = 0$ in Eq. (8):

$$\frac{1}{\bar{c}^2}\frac{\partial^2 p'}{\partial t^2} - \frac{\partial^2 p'}{\partial x^2} = \frac{\gamma - 1}{\bar{c}^2}\frac{\partial q'}{\partial t} \tag{19}$$

The term on the right-hand side describes how the unsteady addition of heat generates pressure disturbances. For a specified rate of heat release, $q'(x,t)$, this inhomogeneous wave equation could be solved to determine the resultant sound field. However, combustion instabilities are due to feedback when the rate of heat release is affected by the flow perturbations it generates. We can illustrate the effects of this through simple model problems.

We again consider a flow that satisfies the boundary conditions (16), but now suppose that the rate of heat release responds to the flow in specified ways.

Example 1. Suppose that the rate of heat release perturbation $q'(x,t)$ is influenced by the local pressure but lags it by a time delay τ. It is convenient to write the constant of proportionality as $2\alpha/(\gamma - 1)$, that is,

$$q'(x,t) = [2\alpha/(\gamma - 1)]p'(x, t - \tau) \tag{20}$$

The form of the pressure perturbation can be determined by substituting for $q'(x,t)$ in (19) and seeking a separable solution, $p'(x,t) = \mathrm{Re}[\hat{p}(x)\exp(i\omega t)]$. This leads, after application of the boundary conditions, to $\hat{p}(x)$ of the form given in Eq. (18), and the equation for the resonant frequency ω is

$$\omega^2 + 2i\omega\alpha\exp(-i\omega\tau) - \omega_n^2 = 0 \tag{21}$$

where ω_n is defined in Eq. (17b).

When $\alpha = 0$, the roots of Eq. (21) are the undamped resonant organ-pipe frequencies ω_n.

When $\alpha \neq 0$ and $\tau = 0$, the quadratic equation (21) for ω can be readily solved to give

$$\omega = -i\alpha \mp \left(\omega_n^2 - \alpha^2\right)^{\frac{1}{2}} \tag{22}$$

Note that ω is now complex. Because the time dependence is $\exp(i\omega t)$, then $-\mathrm{Im}(\omega)$ is the growth rate of the disturbances. Here $\exp(i\omega t) = \exp[\alpha t \mp i(\omega_n^2 - \alpha^2)^{1/2}t]$, showing that the oscillations grow exponentially in time if α is positive. We have recovered Rayleigh's criterion[1] from this particular example: Unsteady heat input in phase with the pressure perturbation has a destabilizing effect and tends to increase the amplitude of the perturbations. In contrast, for negative α, that is, heat input in antiphase with the pressure, the oscillations are damped.

When $\alpha \neq 0$, $\tau \neq 0$, Eq. (21) would, in general, need a numerical solution, and some results are shown in Fig. 2. (In Fig. 2 and subsequently, a normalised frequency $f_N = \mathrm{Re}(\omega)/\omega_1$ and a normalized

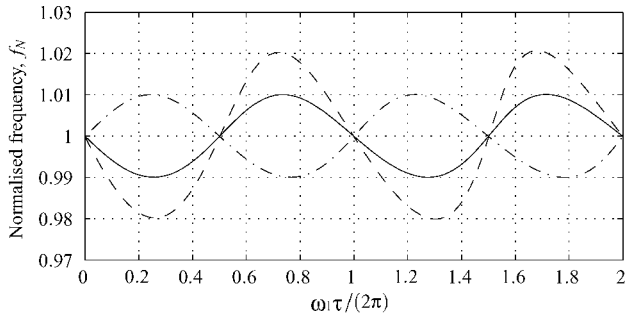

a) Frequency

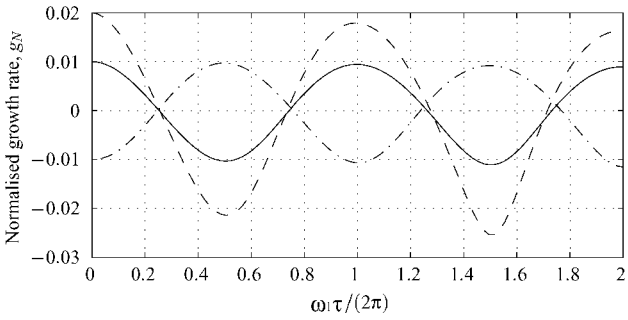

b) Growth rate

Fig. 2 Variation with τ of the root of Eq. (21) near ω_1: ——, $\alpha/\omega_1 = 0.01$; – – –, $\alpha/\omega_1 = 0.02$; and –·–, $\alpha/\omega_1 = -0.01$.

growth rate $g_N = -\mathrm{Im}(\omega)/\omega_1$ are used.) However, the general characteristics of the solution can be investigated by considering small α and determining the roots iteratively. We have already noted that, for $\alpha = 0$, a root of Eq. (21) is at $\omega = \omega_n$. For small α, this root moves to $\omega = \omega_n + \varepsilon$, where ε is small, and substitution into Eq. (21) shows that

$$\varepsilon = -i\alpha \exp(i\omega_n\tau) = -i\alpha\cos(\omega_n\tau) - \alpha\sin(\omega_n\tau) \tag{23}$$

We see from this that any $\alpha\cos(\omega_n\tau) > 0$ leads to a positive growth rate, that is, any unsteady heat input with $-\pi/2 < \mathrm{phase}(\hat{q}/\hat{p}) < \pi/2$ is destabilizing. It is also clear that the resonant frequency is shifted whenever $\alpha\sin(\omega_n\tau) \neq 0$: Rate of heat input in quadrature (∓90 deg) with the pressure alters the frequency, and unsteady rate of heat input leading the pressure (+90 deg) tends to increase the frequency and reduces the frequency when it lags the pressure. This effect was noted by Rayleigh.[1] These analytical predictions for small α are confirmed by the numerical results shown in Fig. 2. For $\alpha > 0$, the growth rate is increased for $\cos(\omega_1\tau) > 0$, that is, $(2n - \frac{1}{2})\pi < \omega_1\tau < (2n + \frac{1}{2})\pi$ and decreased when $\cos(\omega_1\tau)$ is negative. Also the frequency is decreased for $\sin(\omega_1\tau) > 0$ and increased for $\sin(\omega_1\tau) < 0$. The behaviors are reversed for negative α. For nonzero τ, Eq. (21) becomes transcendental and has additional solutions that are primarily related to τ^{-1} rather than the downstream geometry. For example, for small $|\alpha|$ these are at $\mathrm{Im}(\omega) \to \infty$, and $\mathrm{Re}(\omega) \sim 2m\pi/\tau$ for negative α and $(2m+1)\pi/\tau$ for positive α, where m is an integer. We see these are the even/odd harmonics for the convection time τ. The choice of even and odd comes from a balance of the right-hand side and the first term on the left-hand side in Eq. (19), these being much larger than second term on the left-hand side, which represents the axial variation and, hence, the effect of the geometry.

This simple example illustrates that combustion instability is a genuinely coupled problem. Both the acoustics and the unsteady combustion must be considered. The coupling between them affects both the frequency and the susceptibility to self-excited oscillations. At certain conditions, linear perturbances are predicted to grow exponentially with time. In practice, nonlinear effects the most sugnificant of which is usually a saturation in the heat release response (Dowling[14]), lead to a finite amplitude limit cycle oscillation. However, this first example is an oversimplification of what occurs in practice. In LPP gas turbines, it is not the unsteady pressure that has the greatest influence on the rate of heat release: Rather, it is related to the instantaneous fuel–air ratio, which is most affected by the velocity of the airstream near the fuel bars. See the companion paper by Lieuwen[4] for a discussion of the main causes of unsteady combustion. Moreover, the heat release tends to be localized rather than distributed throughout the duct as in example 1. We can again illustrate the influence of these effects through an example.

Example 2. We now consider the unsteady heat input to be concentrated at a single axial plane $x = b$ and to be related to the oncoming air velocity there with a time delay τ,

$$q'(x,t) = Q'(t)\delta(x-b) \tag{24a}$$

$$Q'(t) = -[\beta\bar{\rho}\bar{c}^2/(\gamma-1)]u_1'(t-\tau) \tag{24b}$$

where $Q'(t)$ is the rate of heat input/unit area and subscript 1 denotes conditions just upstream of this region of heat input, that is, $u_1(t) = u(b^-, t)$. Lieuwen[4] discusses forms of the unsteady heat input. In this paper we note that the nondimensional number β can be expected to lie in the range from 0 to about 10 and that in a LPP system τ is typically the convection time from fuel injection to its combustion. (For simplicity, u_1' has been taken to be the velocity just upstream of the flame. However, for consistency with τ being the fuel convection time, the flame model should really be referenced to the perturbations at the fuel injection point, as is done in example 5. However, the distance between these points is typically short compared to the wavelengths, and so the phase difference between them will be small, although they may differ in magnitude by the area ratios.)

With the rate of heat input $q'(x,t)$ as given in Eq. (24a), Eq. (19) reduces to the homogeneous wave equation in the regions $x < b$ and $x > b$. Integration across $x = b$ gives

$$[p']_{x=b^-}^{x=b^+} = 0 \tag{25a}$$

$$\left[\frac{\partial p'}{\partial x}\right]_{x=b^-}^{x=b^+} = -\frac{\gamma-1}{\bar{c}^2}\frac{\mathrm{d}Q'}{\mathrm{d}t} \tag{25b}$$

Equation (25b) is equivalent to

$$[u']_{x=b^-}^{x=b^+} = [(\gamma-1)/\bar{\rho}\bar{c}^2]Q'(t) \tag{26}$$

relating the volumetric expansion to the instantaneous rate of heat input. After substitution for the particular $Q'(t)$ in Eq. (24b), we obtain

$$u'(b_+,t) = u'(b_-,t) - \beta u'(b_-, t-\tau) \tag{27}$$

We will consider solutions with time dependence $\exp(i\omega t)$ and want to find the resonant frequencies ω and the modeshapes.

In $x < b$, the solution of the homogeneous wave equation that satisfies the inlet boundary condition $\hat{p}(0) = 0$ is

$$\hat{p}(x) = A\sin(kx) \tag{28a}$$

$$\hat{u}(x) = (i/\bar{\rho}\bar{c})A\cos(kx) \tag{28b}$$

where k is the wave number $\omega/\bar{c}$ and the complex constant A has yet to be determined. Similarly, in $x > b$, the boundary condition $\hat{u}(l) = 0$ leads to

$$\hat{p}(x) = B\cos[k(l-x)] \tag{29a}$$

$$\hat{u}(x) = (i/\bar{\rho}\bar{c})B\sin[k(l-x)] \tag{29b}$$

The pressure jump condition (25a) then gives

$$A\sin(kb) = B\cos[k(l-b)] \tag{30}$$

whereas the velocity jump condition (27), on division by Eq. (30), gives

$$\tan(kb)\tan[k(l-b)] = 1 - \beta\exp(-i\omega\tau) \tag{31}$$

The resonant frequencies follow from a numerical solution of Eq. (31). Their dependence on β and τ is shown in Figs. 3 and 4.

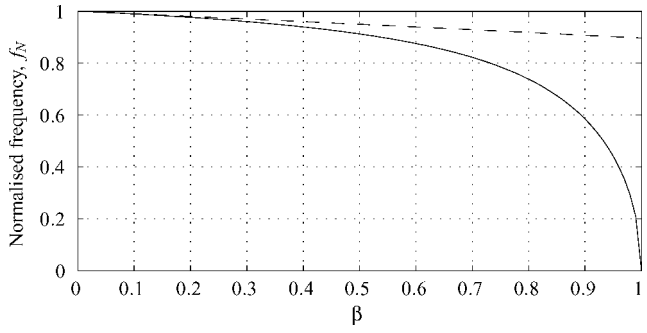

Fig. 3 Variation of frequency with β for the root of Eq. (31) near ω_1, taking $\tau = 0$ and $b = l/10$: ——, exact solution and – – –, one-term Galerkin approximation (40).

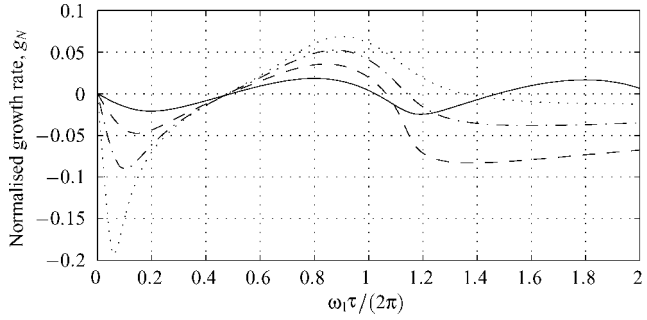

Fig. 4 Variation of growth rate with τ for the root of equation (31) near ω_1, taking $b = l/10$: ——, $\beta = 0.2$; – – –, $\beta = 0.4$; –·–, $\beta = 0.6$; and · · · ·, $\beta = 0.8$.

For $\beta = 0$, the roots are at $\omega = \omega_n$. As β varies, for $\tau = 0$, the rate of heat input is in quadrature with the pressure perturbation and so only shifts the frequency of oscillation: A time lag is required for the unsteady heat input to destabilize the system. [Note the 90-deg phase difference between p' and u' in Eq. (28).] For $\tau \neq 0$, the unsteady heat input affects both the growth rate and the frequency of oscillation. Perturbations grow in time if, in this undamped system, the rate of heat input has a component in phase with pressure perturbation. It is clear from the form of the heat input in Eq. (24b) and the modeshape in Eq. (29) that this requires

$$-\pi < \mathrm{Re}(\omega\tau) - \mathrm{phase}[\beta \cot(kb)] < 0 \tag{32}$$

These bands of instability are clearly seen in Fig. 4.

The modeshapes follow from the substitution for B from Eq. (30) into Eq. (29) and have the form

$$\hat{p}(x) = \begin{cases} C \sin(kx)/\sin(kb) & \text{for} \quad 0 \le x \le b \\ C \cos[k(l-x)]/\cos[k(l-b)] & \text{for} \quad b \le x \le l \end{cases} \tag{33}$$

where the constant C is arbitrary.

Galerkin Series

Another way of solving the inhomogeneous wave equation (19) is through a Galerkin expansion. This involves expanding the pressure perturbation as a Galerkin series:

$$p'(x,t) = \sum_{m=1}^{\infty} \eta_m(t)\psi_m(x) \tag{34}$$

where the functions $\psi_m(x)$ are the eigensolutions or normal modes of the homogeneous wave equation that satisfy the same boundary conditions as p'. In general, they are orthogonal, and we will denote their eigenfrequencies by ω_m. Substitution for the pressure perturbation from Eq. (34) into Eq. (19) then leads to

$$\sum_{m=1}^{\infty} \left(\frac{\mathrm{d}^2\eta_m}{\mathrm{d}t^2} + \omega_m^2 \eta_m \right) \psi_m(x) = (\gamma - 1)\frac{\partial q'}{\partial t} \tag{35}$$

After multiplication by $\psi_n(x)$ and integration with respect to x, the orthogonality of $\psi_n(x)$ shows that Eq. (35) becomes

$$\frac{\mathrm{d}^2\eta_n}{\mathrm{d}t^2} + \omega_n^2\eta_n = \frac{\gamma - 1}{E_n} \int_0^l \frac{\partial q'}{\partial t}\psi_n(x)\,\mathrm{d}x, \qquad n = 1, \ldots \tag{36}$$

where

$$E_n = \int_0^l \psi_n^2\,\mathrm{d}x$$

Equation (36) is a complicated system of equations because $q'(x,t)$ is related to the local flow and so involves all of the unknown coefficients $\eta_m(t)$.

To make the analysis tractable, it is usually assumed that $\partial q'/\partial t$ is small in magnitude and needs only be evaluated approximately. Culick[15] describes the method clearly. When $\partial q'/\partial t = 0$, the nth mode is $\hat{p}(x) = \eta_n(t)\psi_n(x)$ with frequency ω_n. Culick recommends making this acoustic approximation when evaluating $\partial q'/\partial t$, replacing the pressure and velocity perturbations by $\eta_n(t)\psi_n(x)$ and $(\dot{\eta}_n(t)/\bar{\rho}\omega_n^2)\,\mathrm{d}\psi_n/\mathrm{d}x$, respectively, where the dot denotes a time derivative. If the second derivatives of the amplitudes arise, they are replaced by the zeroth-order approximation, $\ddot{\eta}_n(t) \approx -\omega_n^2\eta_n(t)$. The errors introduced by these approximations can be checked by applying the method to find the lowest frequency of oscillation in example 2.

Example 2 by Galerkin series. After applying Culick's rules, the rate of heat release input in Eq. (24) leads to

$$\frac{\partial q'}{\partial t}(x,t) = \frac{\beta\bar{c}^2}{\gamma - 1}\eta_1(t-\tau)\frac{\mathrm{d}\psi_1}{\mathrm{d}x}(b)\delta(x-b) \tag{37}$$

and substitution into Eq. (36) gives

$$\frac{\mathrm{d}^2\eta_1}{t^2} + \omega_1^2\eta_1 = \frac{\beta\bar{c}^2}{E_1}\eta_1(t-\tau)\frac{\mathrm{d}\psi_1}{\mathrm{d}x}(b)\psi_1(b) \tag{38}$$

The solutions ψ_n of the homogeneous wave equation are given in Eq. (18) and $\psi_1(x) = \sin(\pi x/2l)$ leading to $E_1 = \frac{1}{2}l$. Equation (38), therefore, simplifies to

$$\frac{\mathrm{d}^2\eta_1}{\mathrm{d}t^2} + \omega_1^2\eta_1 = \frac{\beta\bar{c}^2\pi}{l^2}\eta_1(t-\tau)\cos\left(\frac{\pi b}{2l}\right)\sin\left(\frac{\pi b}{2l}\right) \tag{39}$$

The frequency of oscillation, ω, can be found by substituting $\eta_1(t) = C\exp(i\omega t)$ into Eq. (39) to give

$$\omega^2 = \omega_1^2 - (\beta\bar{c}^2\pi/2l^2)\exp(-i\omega\tau)\sin(\pi b/l) \tag{40}$$

The root of this equation is shown as a dashed line in Fig. 3 for the particular case $\tau = 0$. Comparison with the exact solution given in Eq. (31) shows that the one-term Galerkin expansion gives the correct frequency and gradient at $\beta = 0$ but that it rapidly diverges from the exact solution as β increases. That is not really surprising: This method treats the shift in frequency as small, but it can be substantial for the type of combustion response typical of LPP systems. The inadequacy of the one-term Galerkin for a more complicated model problem was discussed by Dowling.[16] Annaswamy et al.[17] noted that three terms in the Galerkin series were needed to model the system dynamics for feedback control.

With Temperature Gradients

So far our examples have been somewhat artificial: They have had an unsteady heat input $q'(x,t)$ and yet the mean temperature has been uniform. In practice, of course, heat input is associated with temperature gradients and the mean temperature and density are functions of position. We will introduce these effects through discussion of the zero mean flow case. Then the momentum equation (1b) ensures that the mean pressure is uniform and for linearized perturbations,

$$\bar{\rho}\frac{\partial \boldsymbol{u}'}{\partial t} = -\nabla p' \tag{41}$$

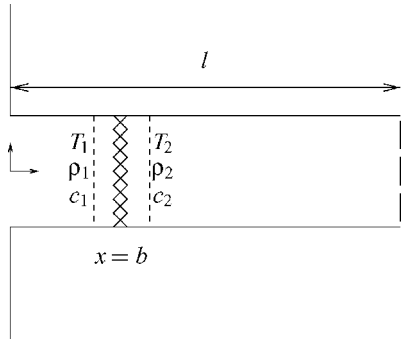

Fig. 5 System for example 3.

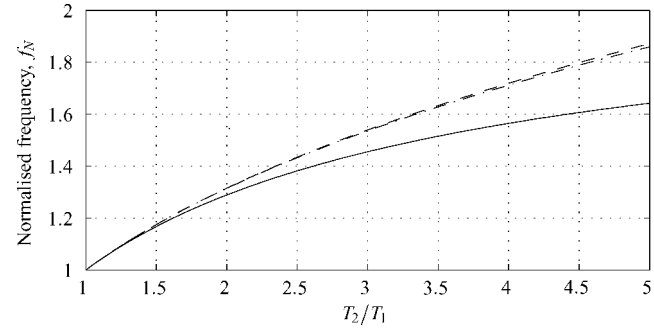

Fig. 6 Variation of frequency with mean temperature ratio for solution near ω_1 taking $\beta = \tau = 0$ and $b = l/10$: ——, root of Eq. (47), that is solution for single temperature jump at $x = b$; – – –, uniformly distributed heat release between $x = 0$ and $x = 2b$ approximated by 10 temperature jumps; and –·–, uniformly distributed heat release between $x = 0$ and $x = 2b$ approximated by 5 temperature jumps.

in an inviscid flow. We show in the Appendix that the mass conservation equation (1a) and the entropy equation (4) can be combined to give

$$\frac{1}{\bar{\rho}\bar{c}^2}\frac{\partial p'}{\partial t} = \nabla \cdot \boldsymbol{u}' + \frac{\gamma - 1}{\bar{\rho}\bar{c}^2} q' \tag{42}$$

when heat conduction and viscous effects are neglected. Eliminating $\boldsymbol{u}'$ from Eqs. (41) and (42), we obtain

$$\frac{1}{\bar{c}^2}\frac{\partial^2 p'}{\partial t^2} - \bar{\rho}\nabla \cdot \left(\frac{1}{\rho}\nabla p'\right) = \frac{\gamma - 1}{\bar{c}^2}\frac{\partial q'}{\partial t} \tag{43}$$

In this equation, $\bar{\rho}$ and $\bar{c}$ vary with position, but $\bar{\rho}\bar{c}^2 = \gamma\bar{p}$ is uniform if the small dependence of γ on temperature is neglected. We can illustrate the influence of temperature variation by extending example 2 to the case where the mean temperature rises from $\bar{T}_1$ to $\bar{T}_2$ across the zone of heat input at $x = b$, with corresponding changes in sound speed and density.

Example 3. Consider one-dimensional linear disturbances of frequency ω in the system shown in Fig. 5. Just as in example 2, we again apply the boundary conditions (16) and the flame model (24).

Outside the flame zone $x = b$, the solutions of the homogeneous wave equation (43), satisfying the appropriate boundary conditions, have the same form as in example 2 provided the local mean flow variables are used. Hence, using Eqs. (28) and (29), we can write in $x < b$

$$\hat{p}(x) = A\sin(k_1 x) \tag{44a}$$

$$\hat{u}(x) = (i/\bar{\rho}_1\bar{c}_1)A\cos(k_1 x) \tag{44b}$$

and in $x > b$

$$\hat{p}(x) = B\cos[k_2(l - x)] \tag{44c}$$

$$\hat{u}(x) = [i/\bar{\rho}_2\bar{c}_2]B\sin[k_2(l - x)] \tag{44d}$$

where $k_1 = \omega/\bar{c}_1$ and $k_2 = \omega/\bar{c}_2$.

Integration of Eq. (43) with $q'(x, t) = Q'(t)\delta(x - b)$ across the region $x = b$ leads to

$$[p']_{x=b^-}^{x=b^+} = 0 \tag{45a}$$

$$\left[\frac{1}{\rho}\frac{\partial p'}{\partial x}\right]_{x=b^-}^{x=b^+} = -\frac{\gamma - 1}{\bar{\rho}_1\bar{c}_1^2}\frac{\mathrm{d}Q'}{\mathrm{d}t} \tag{45b}$$

Equation (45b) is equivalent to

$$[u']_{x=b^-}^{x=b^+} = \frac{\gamma - 1}{\bar{\rho}_1\bar{c}_1^2}Q'(t) \tag{46}$$

After substituting for the particular $Q'(t)$ in Eq. (24b) and using Eq. (44), we obtain

$$\tan(k_1 b)\tan[k_2(l - b)] = (\bar{\rho}_2\bar{c}_2/\bar{\rho}_1\bar{c}_1)[1 - \beta\exp(-i\omega\tau)] \tag{47}$$

A comparison with Eq. (31) shows that the varying temperature effects appear not only in the wave numbers k_1 and k_2, which account for propagation effects, but also in the factor $\bar{\rho}_2\bar{c}_2/(\bar{\rho}_1\bar{c}_1)$, which describes the impedance change across the flame zone. The solid line in Fig. 6 shows how the temperature variations affect the resonant frequency. A typical LPP gas turbine combustor operates with a temperature ratio of around 3 ($\bar{T}_1 \sim 700$ K and $\bar{T}_2 \sim 2000$ K).

So far we have assumed that the flame is compact, that is, axially short compared the wavelengths of the perturbations. If this is not the case, we may approximate the axial heat release distribution by discretizing into a series of compact flames, each having the form described earlier. Between these, there is assumed to be no heat release, and so we use the usual wave propagation (15). The dashed and dashed–dotted lines in Fig. 6 show results for applying this approximation when, instead of a compact flame at $x = b$, we have a uniformly distributed heat release between $x = 0$ and $x = 2b$. It leads to a 6% shift in the frequency at a temperature ratio 3. An alternative approach is to seek a continuous analytical solution. Exact solutions can be found for particular temperature distributions (such as linear variations and power laws)[18–23] and also for certain area variations.[24,25]

Effect of a Mean Flow

Most combustion systems involve a mean flow that brings fresh reactants into the combustion zone. The Mach number of the oncoming flow is so small (typically less than 0.1) that it is tempting to neglect this mean velocity. The errors introduced by such an approximation are investigated in this section.

A mean flow has two main consequences. Trivially, it affects the speed of propagation of the acoustic waves, with one-dimensional disturbances then traveling downstream with speed $\bar{c} + \bar{u}$ and upstream at $\bar{c} - \bar{u}$. In addition, the mean flow admits the possibility of convected entropy and vorticity disturbances. These modes are coupled by the requirement of conservation of mass, momentum, and energy across zones of heat input.

Example 4. These effects may be illustrated by extending example 2 to include a mean flow. For definiteness we again apply an open-end inlet boundary condition $p'(0) = 0$. At the downstream end, we assume an area restriction in which the flow becomes choked, that is, the mean flow velocity accelerates to the local speed of sound. This is approximately the case for gas turbine combustors where the nozzle guide vanes at entry to the turbine are choked. The appropriate boundary condition is then one of constant nondimensional mass flow, or equivalently, constant Mach number. For linear perturbations, this reduces to

$$2(u'/\bar{u}) + \rho'/\bar{\rho} - p'/\bar{p} = 0 \tag{48}$$

(as discussed already in the boundary conditions section). Note that the hard end boundary condition $u' = 0$ is recovered from Eq. (48) as $\bar{u}$ tends to zero. The heat input will again be considered as concentrated at the fixed plane $x = b$, the rate of heat input per unit cross-sectional area being denoted by $Q'(t)$ with $Q'(t)$ given by the particular flame model in Eq. (24).

Upstream of the zone of heat input, there are acoustic waves propagating in both directions, and the flow is isentropic. The pressure perturbation is the general solution of the convected wave equation (9); this gives

$$p'(x,t) = A\exp(i\omega t)\big(\exp\{-i\omega x/[\bar{c}_1(1+\bar{M}_1)]\} - \exp\{i\omega x/[\bar{c}_1(1-\bar{M}_1)]\}\big) \quad (49)$$

for disturbances of frequency ω, $\bar{M}_1 = \bar{u}_1/\bar{c}_1$. For this isentropic flow, $\rho' = p'/\bar{c}_1^2$, and for a perfect gas, $c_p T' = p'/\bar{\rho}$. The velocity fluctuation follows directly from the momentum equation (7b):

$$\bar{\rho}_1\bar{c}_1 u'(x,t) = A\exp(i\omega t)\big(\exp\{-i\omega x/[\bar{c}_1(1+\bar{M}_1)]\} + \exp\{i\omega x/[\bar{c}_1(1-\bar{M}_1)]\}\big) \quad (50)$$

The fluxes of mass, momentum, and stagnation enthalpy into the combustion zones [defined in Eq. (10)] can be expressed in terms of the unknown complex A through Eqs. (49) and (50).

Downstream of the region of heat input, there might be a convected hot spot in addition to plane sound waves, and so

$$p'(x,t) = \exp(i\omega t)\big(C\exp\{-i\omega x/[\bar{c}_2(1+\bar{M}_2)]\} + D\exp\{i\omega x/[\bar{c}_2(1-\bar{M}_2)]\}\big) \quad (51a)$$

$$\bar{\rho}_2\bar{c}_2 u'(x,t) = \exp(i\omega t)\big(C\exp\{-i\omega x/[\bar{c}_2(1+\bar{M}_2)]\} - D\exp\{i\omega x/[\bar{c}_2(1-\bar{M}_2)]\}\big) \quad (51b)$$

$$\rho'(x,t) = \left[p'(x,t)\Big/\bar{c}_2^2\right] - (S\bar{\rho}_2/c_p)\exp[i\omega(t-x/\bar{u}_2)] \quad (51c)$$

$$c_p T'(x,t) = [p'(x,t)/\bar{\rho}_2] + \left[S\bar{c}_2^2\Big/(\gamma-1)c_p\right]\exp[i\omega(t-x/\bar{u}_2)] \quad (51d)$$

for $b \le x \le l$ and $\bar{M}_2 = \bar{u}_2/\bar{c}_2$. C and D are the amplitudes of the acoustic waves, S is that of the entropy wave or convected hot spot, and there are no vorticity waves in this one-dimensional example. The wave amplitudes C, D, and S can be found in terms of A through Eqs. (10a–10c), which are the statement of conservation of mass, momentum, and energy flow across the flame zone:

$$\rho_2 u_2 = \rho_1 u_1 \quad (10a)$$

$$p_2 + \rho_2 u_2^2 = p_1 + \rho_1 u_1^2 \quad (10b)$$

$$\rho_2 u_2 H_2 = \rho_1 u_1 H_1 + Q_A \quad (10c)$$

where $H = c_p T + \frac{1}{2}u^2$ is the stagnation enthalpy and suffixes 1 and 2 denote conditions just upstream and downstream of the flame zone, respectively, that is, at $x = b_-$ and b_+.

Care needs to be taken to recover the jump conditions for zero mean flow from Eq. (10). In the limit $\bar{u}_1, \bar{u}_2 \to 0$, Eq. (10b) clearly simplifies to $p_2 = p_1$, the zero mean flow jump condition [Eqs. (25a) and (45a)]. At first sight one might assume that Eq. (10a) gives $\bar{\rho}_2 u_2' = \bar{\rho}_1 u_1'$ as $\bar{u}_1, \bar{u}_2$ tend to zero. That is wrong: Note it is incompatible with Eq. (46). The resolution of this apparent inconsistency is that the strength of the entropy wave S enters the jump conditions (10) only in the product $\bar{u}_2 S$. In the limit $\bar{u}_2 \to 0$, S tends to infinity, in such a way as to keep the product $\bar{u}_2 S$ and, hence, $\bar{u}_2\rho_2'$ and $\bar{u}_2 T_2'$, finite. For low Mach number mean flows, there are very large entropy fluctuations downstream of the flame zone. To see this mathematically, it is convenient to first use Eq. (10a) to recast Eq. (10c) into the form

$$\bar{\rho}_2\bar{u}_2(c_p T_2' + \bar{u}_2 u_2') = Q' + \bar{\rho}_1\bar{u}_1(c_p T_1' + \bar{u}_1 u_1') - (\bar{H}_2 - \bar{H}_1)(\bar{\rho}_1 u_1' + \rho_1'\bar{u}_1) \quad (52)$$

for linear perturbations. After Eq. (51d) is used to expand $c_p T_2'$ and the limit $\bar{u} \to 0$ is taken, this simplifies to

$$\frac{\bar{\rho}_2\bar{u}_2\bar{c}_2^2}{c_p(\gamma-1)} S\exp\left[i\omega\left(t-\frac{b}{\bar{u}_2}\right)\right] = Q' - c_p(\bar{T}_2 - \bar{T}_1)\bar{\rho}_1 u_1' \quad (53)$$

Physically, Eq. (53) shows that entropy is generated unsteadily at the combustion zone whenever $Q' \neq c_p(\bar{T}_2 - \bar{T}_1)\bar{\rho}_1 u_1'$, that is, whenever there is unsteadiness in the rate of heat addition per unit mass. In particular, the assertion above that $\bar{u}S$ remains finite for small $\bar{u}$ is confirmed. It is clear from Eq. (51c) that, in this limit, the left-hand side of Eq. (53) is equal to $-\bar{u}_2\bar{c}_2^2\rho_2'/(\gamma-1)$, and hence, the equation can be rearranged to give

$$\bar{u}_2\rho_2' = -\left[(\gamma-1)\Big/\bar{c}_2^2\right]Q' + (\bar{\rho}_1 - \bar{\rho}_2)u_1' \quad (54)$$

where we have used the perfect gas relationships to rewrite $c_p(\gamma-1)(\bar{T}_2 - \bar{T}_1)\bar{\rho}_1/\bar{c}_2^2$ as $\bar{\rho}_1 - \bar{\rho}_2$. Finally, substitution for $\bar{u}_2\rho_2'$ in the equation of mass conservation leads to

$$\bar{\rho}_2 u_1' = \bar{\rho}_2 u_2' - \left[(\gamma-1)\Big/\bar{c}_2^2\right]Q' \quad (55)$$

thereby recovering the zero mean flow jump condition (46).

Once Q' has been related to the unsteady flow by a flame model and linear flow perturbations expressed in terms of waves, the three equations describing conservation of mass, momentum, and energy across the flame zone can be rearranged to determine the downstream wave amplitudes C, D, and S in terms of the upstream wave amplitude A.

With the wave amplitudes known, the flow perturbation at any position in the duct can be written down using Eq. (51). For a general value of ω, the flow will not satisfy the exit boundary condition (48). It is, therefore, necessary to iterate in ω to find the complex values of ω for which the exit boundary condition is met. These are the frequencies of the thermoacoustic oscillations. Only disturbances with these particular frequencies can exist as free modes of the duct/flame. The modes shapes are determined in this linear theory, but not the level of the oscillation. In other words, a single wave amplitude, for example, A, is arbitrary, but then all other wave amplitudes are given in terms of A.

Combustion usually occurs in a low Mach number flow, and $2\pi\bar{u}_2/\omega$, the wavelength of the entropy wave, can be very short indeed for high-frequency disturbances. Then turbulent mixing and diffusion tend to smooth out the entropy fluctuations as they convect downstream. As a consequence, although a strong entropy fluctuation may be generated in the flame zone, the amplitude of a high-frequency entropic disturbance may be negligible by the time the wave reaches the exit of the combustor. Judgment is needed, based on the ratio of mixing to convection time, to decide whether the entropy waves persist as far as the downstream contraction. If they do not, ρ' should be replaced by its acoustic contribution $p'/\bar{c}^2$ in the downstream boundary condition (48). We would expect the entropy fluctuations to only be of importance for the lowest-frequency acoustic mode, if at all. Figure 7 shows the effects of a mean flow on the lowest acoustic mode of oscillation when the entropy wave has diffused before the exit contraction. The frequency varies only very slightly with Mach number, that is, the variation is order Mach number squared and is 5% at a Mach number of 0.2.

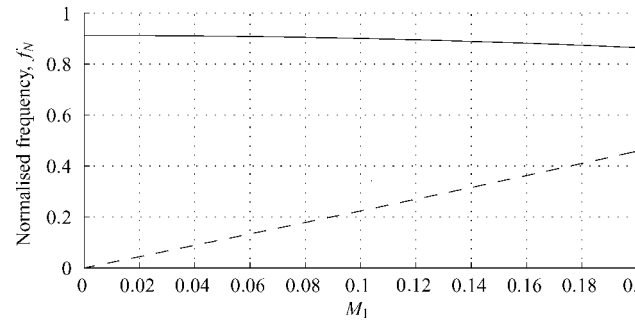

Fig. 7 Variation of frequency with Mach number for lowest-frequency mode, taking $\bar{Q} = 0$: ——, acoustic mode when diffusion attenuates the entropy waves by the combustor exit, hence mode is near ω_1 and – – –, including entropy waves, hence mode is a low-frequency convection mode.

An additional consequence of a mean flow is that it admits a different mode of oscillation, one with a much lower resonance frequency (typically 40–150 Hz for aeroengines), where the period of oscillation is set by the convection time of the entropy fluctuations from the flame zone to the exit nozzle and the propagation of an acoustic wave back upstream (see Zhu et al.[26]). This acoustic wave causes unsteady combustion through its effect on the inlet velocity. The unsteady combustion leads to entropy waves or local hot spots. At these low frequencies, the entropy wavelengths are long and the waves undergo little attenuation, generating sound as they are convected through the downstream contraction. The acoustic wave propagates back upstream, thus, completing the cycle. Only the first few harmonics of this type of mode will be present because, as already discussed, at higher frequencies the entropy waves will diffuse. An example of such a convection mode is shown as a dashed line in Fig. 7. We see that the frequency is approximately proportional to the Mach number.

In this section, we have introduced some of the parameters that affect one-dimensional acoustic waves in gas turbine combustors. In many industrial gas turbines, where the combustors are long, the most unstable modes are indeed plane, but even these combustors support more complex modal solutions. Aeroengine combustors are often annular with a short axial length. Then the lowest frequency (and often the most unstable) modes are associated with circumferential waves. We discuss these more general modes in the next section.

Modal Solutions

We now consider perturbations that are three dimensional. We consider two geometries relevant to gas turbines, first, a cylindrical duct and, second, an annular duct. Particular attention is given to the special case of the latter geometry when the annular gap is small: This limit often occurs in practical applications, and the acoustic waves then have a particularly simple form.

Cylindrical Duct

Using cylindrical polar coordinates x, r, and θ, we are interested in a straight cylindrical duct, $0 \le r \le b$. Because we are assuming that the mean flow is uniform, we must have $\bar{v} = \bar{w} = 0$. We look for separable solutions for the three types of disturbance mentioned earlier. The general solution is a sum of such separable solutions.

We first consider a pressure disturbance. We seek a separable solution by substituting $p' = F(t)X(x)\ B(r)\Theta(\theta)$ into Eq. (9) to give

$$\frac{F''}{F} + 2\bar{u}\frac{F'X'}{FX} + \bar{u}^2\frac{X''}{X} - \bar{c}^2\left(\frac{X''}{X} + \frac{(rB')'}{rB} + r^{-2}\frac{\Theta''}{\Theta}\right) = 0 \quad (56)$$

where the prime denotes a derivative with respect to the argument. We see that solutions take the form $F(t) = \exp(i\omega t)$, $X(x) = \exp(ikx)$, and $\Theta(\theta) = \exp(in\theta)$, with

$$(rB')' + (\lambda^2 - n^2 r^{-2})rB = 0 \quad (57)$$

where $\lambda^2 = (\omega + \bar{u}k)^2/\bar{c}^2 - k^2$. For continuity in θ, the circumferential wave number n must be an integer. The axial wave number k and complex frequency ω may take any complex value, but they are dependent. The general solution of Eq. (57) is $B(r) = c_1 J_n(\lambda r) + c_2 Y_n(\lambda r)$, where J_n and Y_n are the Bessel functions of the first and second kind, respectively. Because Y_n is singular at $r = 0$, we must have $c_2 = 0$, and the rigid-wall boundary condition $v(b) = 0$ implies

$$\frac{\mathrm{d}J_n}{\mathrm{d}r}(\lambda b) = 0 \quad (58)$$

For a given n, this gives an infinite number of discrete solutions for λ. The solutions are all real,[27] and without loss of generality we may take $\lambda \ge 0$. We define $\lambda_{n,m}$ to be the $(m+1)$th solution. The full solution can be expressed as an acoustic wave of the form[28]

$$p' = A_\pm \exp(i\omega t + in\theta + ik_\pm x) B_{n,m}(r) \quad (59a)$$

$$\rho' = \frac{1}{\bar{c}^2} A_\pm \exp(i\omega t + in\theta + ik_\pm x) B_{n,m}(r) \quad (59b)$$

$$u' = -\frac{k_\pm}{\bar{\rho}\alpha_\pm} A_\pm \exp(i\omega t + in\theta + ik_\pm x) B_{n,m}(r) \quad (59c)$$

$$v' = \frac{i}{\bar{\rho}\alpha_\pm} A_\pm \exp(i\omega t + in\theta + ik_\pm x) \frac{\mathrm{d}B_{n,m}}{\mathrm{d}r}(r) \quad (59d)$$

$$w' = -\frac{n}{r\bar{\rho}\alpha_\pm} A_\pm \exp(i\omega t + in\theta + ik_\pm x) B_{n,m}(r) \quad (59e)$$

with $B_{n,m}(r) = J_n(\lambda_{n,m} r)$. [Note that the perturbations as given in Eq. (59) will be complex, but it is assumed that we take the real part.] Here $\alpha_\pm = \omega + \bar{u}k_\pm$,

$$k_\pm = \frac{\bar{M}\omega \mp \left(\omega^2 - \omega_c^2\right)^{\frac{1}{2}}}{\bar{c}(1 - \bar{M}^2)} \quad (60)$$

and $\bar{M}$ is the mean Mach number (which is assumed to be less than unity). Also $\omega_c = \bar{c}\lambda_{n,m}(1 - \bar{M}^2)^{1/2}$ is the complex cutoff frequency of the duct, and $A_\pm$, which may be complex, are the wave amplitudes. For real $\omega > \omega_c$, A_+ is a downstream-propagating wave and A_- is an upstream-propagating wave. For real $\omega < \omega_c$ the waves are cutoff. Defining the square root in Eq. (60) to be a negative imaginary number, A_+ is now a downstream-decaying disturbance and A_- is an upstream-decaying disturbance. For complex ω, a combination of these behaviors is seen.

The separable solutions for an entropy disturbance are entropy waves of the form

$$\rho' = -(1/\bar{c}^2) A_E \exp(i\omega t + in\theta + ik_0 x) E(r) \quad (61)$$

with $p' = u' = v' = w' = 0$, where $k_0 = -\omega/\bar{u}$ and $E(r)$ can be any function of r. For a vorticity disturbance, the solution can be thought of as a sum of two types of vorticity wave, one where the radial velocity is zero and one where the circumferential velocity is zero.[13] The first type has the form

$$u' = (n/\bar{\rho}\bar{c}) A_V \exp(i\omega t + in\theta + ik_0 x) V(r) \quad (62a)$$

$$w' = -(k_0 r/\bar{\rho}\bar{c}) A_V \exp(i\omega t + in\theta + ik_0 x) V(r) \quad (62b)$$

with $p' = \rho' = v' = 0$, whereas perturbations in the second type can be expressed as

$$u' = \frac{1}{\bar{\rho}\bar{c}r} A_W \exp(i\omega t + in\theta + ik_0 x) \frac{\mathrm{d}W}{\mathrm{d}r}(r) \quad (63a)$$

$$v' = -\frac{ik_0}{\bar{\rho}\bar{c}r} A_W \exp(i\omega t + in\theta + ik_0 x) W(r) \quad (63b)$$

with $p' = \rho' = w' = 0$. The only restrictions on $V(r)$ and $W(r)$ are that $V(0) = W(0) = W(b) = 0$.

In this section we have assumed that the duct wall is rigid. The case of a compliant duct wall is discussed by Eversman,[28] as is the case of a nonuniform mean flow.

Annular Duct

Many gas turbines, particularly aeroengines, have an annular geometry. Hence, we will now consider the form of perturbations that can occur in the gap between two rigid-walled concentric cylinders $a \le r \le b$. The acoustic waves are the same as for a cylindrical duct except that now[29]

$$B_{n,m}(r) = \frac{\mathrm{d}Y_n}{\mathrm{d}r}(\lambda_{n,m} b) J_n(\lambda_{n,m} r) - \frac{\mathrm{d}J_n}{\mathrm{d}r}(\lambda_{n,m} b) Y_n(\lambda_{n,m} r) \quad (64)$$

and $\lambda_{n,m} \ge 0$ is now the $(m+1)$th solution of

$$\frac{\mathrm{d}J_n}{\mathrm{d}r}(\lambda_{n,m} a)\frac{\mathrm{d}Y_n}{\mathrm{d}r}(\lambda_{n,m} b) = \frac{\mathrm{d}J_n}{\mathrm{d}r}(\lambda_{n,m} b)\frac{\mathrm{d}Y_n}{\mathrm{d}r}(\lambda_{n,m} a) \quad (65)$$

from the rigid-wall boundary conditions on $r = a$ and $r = b$. [Using a similar approach to that given by Watson[27] to prove that J_n only has real zeros, it can be shown that the solutions of Eq. (64) are again all real.] The entropy waves are unchanged. For the vorticity waves, there is now no restriction on the function $V(r)$, whereas for $W(r)$ we have $W(a) = W(b) = 0$.

Narrow Annular Gap

In annular gas turbines, the radial gap of the combustor is typically shorter than the axial length and much shorter than the circumference. In such situations, we may approximate the flow by considering the case when the annular gap is narrow, that is, $a \approx b$. For $m = 0$, $B_{n,0}(r)$ can be approximated as constant; hence, in particular $v' = 0$, and it can be shown that $\lambda_{n,0} \approx n/R$, where $R = \frac{1}{2}(a + b)$. The higher-order radial modes, $m > 0$, are highly cut off (meaning that they have rapid axial decay) and can be ignored. (Comparison with full solutions confirms the expected radial independence.) For the entropy and vorticity waves, $E(r)$ and $V(r)$ should be taken to be constant whereas $W(r)$ should be discarded. (For more details on this approximation and its applicability see Stow et al.[13])

We now illustrate modal solutions, specifically, circumferential modes in a narrow annular gap, with an example. As before we consider a uniform straight duct, length l. However, we now impose a mean flow and change the inlet and outlet boundary conditions to be choked. Also, we assume the duct to have a narrow annular cross section. Entropy waves (and vorticity waves if $n \neq 0$) will be generated at the inlet and convected with the mean flow to the outlet where they can interact with the acoustic waves. However, because the entropy and vorticity waves have a short wavelength [see Eqs. (61–63)], if the duct is long they are likely to be diffused away by mixing processes before they reach the combustor outlet. Hence, initially we ignore the influence of these waves at the downstream boundary. When the Mach number in the duct is taken to be small, the choked inlet and outlet boundary conditions give $u' \approx 0$. Hence, for plane waves, $n = 0$, the resonant modes of the duct for integer m are approximately the organ-pipe resonances,

$$\omega \approx \tilde{\omega}_m = m\pi\bar{c}/l \tag{66a}$$

$$\hat{p}(x) \approx A_m \cos(m\pi x/l) \tag{66b}$$

$$\hat{u}(x) \approx -(iA_m/\bar{\rho}\bar{c}) \sin(m\pi x/l) \tag{66c}$$

where we have taken $p'(t, x, \theta) = \hat{p}(x) \exp(i\omega t + in\theta)$. For circumferential waves, $n \neq 0$, for integer m, ω is given by

$$\omega \approx \left(\tilde{\omega}_m^2 + \omega_c^2\right)^{\frac{1}{2}} \tag{67}$$

where $\omega_c = n\bar{c}/R$ is the cutoff frequency of the duct, with the mode-shapes also approximated by Eqs. (66b) and (66c). In particular, for a given n the lowest frequency mode is close to the cutoff frequency and has a pressure perturbation that is roughly uniform axially. The frequencies [$= \mathrm{Re}(\omega)/(2\pi)$] and growth rates [$= -\mathrm{Im}(\omega)$] of the modes for $n = 0$ and 1 are shown as circles in Fig. 8. The pressure distribution for the second $n = 1$ mode at a sequence of times in its oscillation period ($T = 1/\text{frequency}$) is shown in Fig. 9. Axially the mode is a standing half-wave, whereas circumferentially it is a spinning whole wave. All of the modes have negative growth rate. This is because the choked inlet and choked outlet boundary conditions do not give a perfect reflection of acoustic waves and are, therefore, a

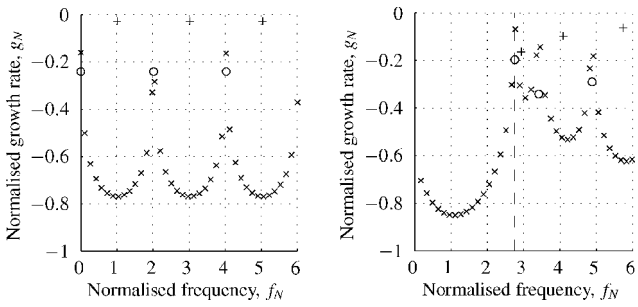

a) $n = 0$ **b) $n = 1$**

Fig. 8 Frequencies and growth rates of resonate modes of a duct with choked outlet: ×, choked inlet with entropy and vorticity waves included; ○, choked inlet with entropy and vorticity waves assumed to be dissipate before combustor exit; +, open inlet (hence, no entropy and vorticity waves); and – – –, cutoff frequency of the duct for $n = 1$.

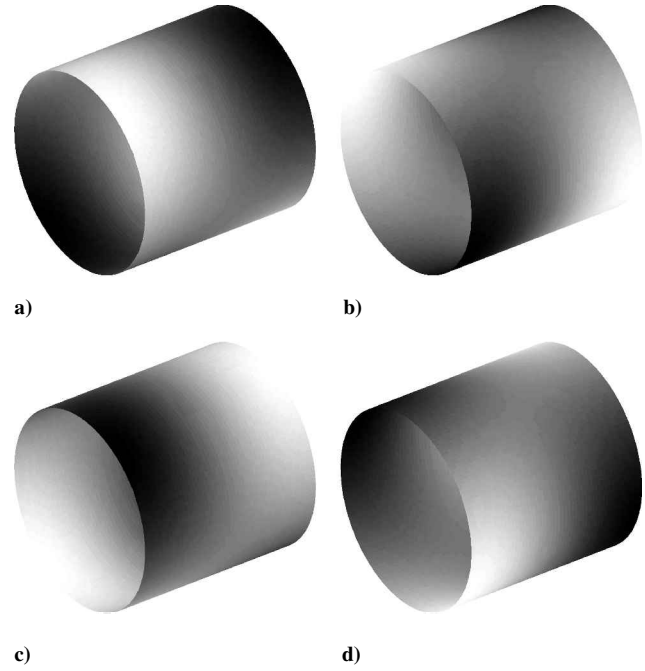

a) **b)** **c)** **d)**

Fig. 9 Time sequence of pressure distribution in thin annular duct for second mode in Fig. 8b (choked–choked configuration with dissipation of entropy and vorticity). Light indicates pressure greater than the mean, that is, positive perturbation, and dark indicates negative pressure perturbation (arbitrary scale): a) $t = 0$; b) $t = T/4$; c) $t = T/2$; and d) $t = 3T/4$.

sources of damping. If entropy and vorticity wave propagation is included, many more modes are found, as denoted by crosses in Fig. 8. The modes are roughly $\bar{u}/(2l)$ Hz apart, that is, $\mathrm{Re}(\Delta\omega) \approx \pi\bar{u}/l$. The least stable modes, that is, those with the largest growth rates, are found to be close to the modes when entropy and vorticity waves are ignored. For comparison with the earlier examples, results for an open inlet/choked outlet are shown as pluses in Fig. 8. As we would expect, the frequencies lie midway between the choked inlet/choked outlet frequencies. In this case, neither entropy nor vorticity waves are generated by the open inlet and so neither are present in the duct. Also, the growth rates are less negative here because the open inlet gives no damping.

Application to Gas Turbine Combustors

So far, we have described the modal analysis of simple cylindrical and annular ducts and shown how, with appropriate boundary conditions, it leads to their resonant frequencies. However, the geometry of gas turbine combustors is far from simple. The acoustics of the gas turbine from compressor exit to turbine entry may play a role in combustion instability. A typical geometry is shown in Fig. 10.

The high-speed flow at the compressor exit is slowed down in a diffuser and made more uniform in preparation for fuel addition and combustion. At the downstream end of the diffuser, the air is accelerated through premixing ducts, where fuel is added, and the premixed fuel and air then enter a combustion chamber, where it is burnt. Although this geometry is complex, it is made up of a series of annular and cylindrical ducts: The flow passage is annular at compressor exit, the premix ducts have small cross-sectional areas in which only one-dimensional waves propagate, and the combustion chamber may be either annular or cylindrical. Our earlier analysis is, therefore, relevant provided we know how to join ducts of different cross-sectional areas. We can illustrate the approach by discussing the simple quasi-one-dimensional geometry in Fig. 11.

Acoustics of the Diffuser/Plenum

We investigate the form of linear disturbances in the geometry of a plenum section, premixing ducts, and combustor. In this example, we will assume that the frequency of oscillation is sufficiently low

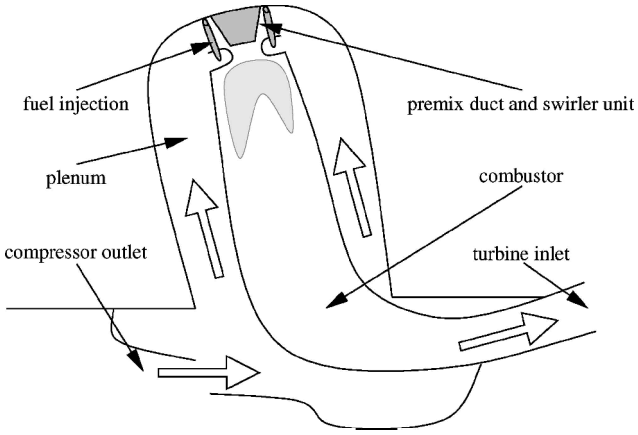

Fig. 10 Typical gas turbine geometry.

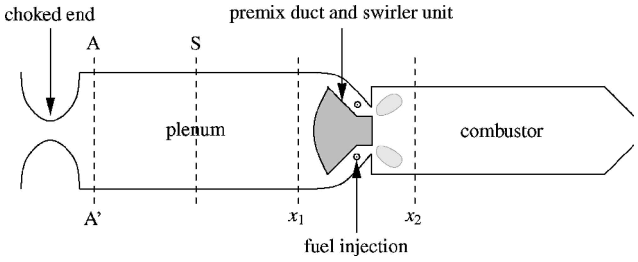

Fig. 11 Simple quasi-one-dimensional combustor.

that only plane waves carry acoustic energy, with all higher-order modes decaying exponentially with axial distance.

At the inlet, representing compressor exit, the flow is nearly choked. This means that the mass and energy flow rates are nearly constant irrespective of downstream pressure perturbations and (as discussed in boundary conditions section earlier) this leads to inlet boundary conditions for the linear waves of frequency ω. The relative wave strengths at A–A' (Fig. 11) are then completely determined.

Equations (7c), (7d), and (9) describe how those wave develop along the plenum, hence, determining the unsteady flow at entrance to the premix duct.

Joining Plenum and Combustor

There are two main approaches to relating the perturbations in the plenum and combustor: One is purely acoustic and often relies on empirical inputs, whereas the second is model based through appropriate application of the equations of conservation of mass, momentum, and energy.

The acoustic approach involves determination from experiment[30] or simple models[31,32] of the transfer matrix $\boldsymbol{N}(\omega)$, which relates pressure and velocity perturbations at the entrance to the premixer (denoted by subscript 1) to perturbations downstream of the combustion zone (denoted by subscript 2):

$$\begin{bmatrix} \hat{p}_1 \\ \hat{u}_1 \end{bmatrix} = \boldsymbol{N}(\omega) \begin{bmatrix} \hat{p}_2 \\ \hat{u}_2 \end{bmatrix} \tag{68}$$

(A schematic diagram is shown in Fig. 12.) The 2×2 matrix $\boldsymbol{N}$ depends on the details of the geometry and the flow between x_1 and x_2. For example, for the duct with uniform cross-sectional area, and a flow with negligible mean flow and the flame model in Eq. (24b), we found [see Eqs. (25a) and (27)]

$$\boldsymbol{N} = \begin{bmatrix} 1 & 0 \\ 0 & [1 - \beta \exp(-i\omega\tau)]^{-1} \end{bmatrix} \tag{69}$$

In the case where the premix duct is short and has small cross-sectional area and there is no combustion, the flow in the premix duct is effectively incompressible, and the pressure difference across it can be related to the rate of change of momentum in the premix duct. For negligible mean flow, the relationship is $A_3(\hat{p}_1 - \hat{p}_2) = (\partial/\partial t)(AL\rho u)_3 = i\omega\bar{\rho}A_3L_3\hat{u}_3$, where A is the cross-sectional area and L the effective axial length, suffix 3 denoting flow within the premix duct. From conservation of mass, $A_1\hat{u}_1 = A_2\hat{u}_2 = A_3\hat{u}_3$. Hence, we have

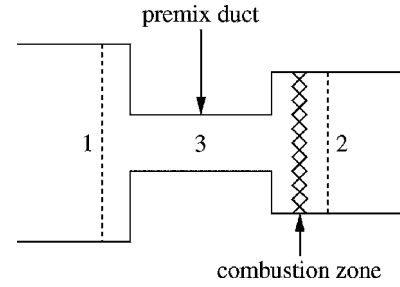

Fig. 12 Schematic diagram of premix duct and combustion zone (for definition of transfer matrix).

$$\boldsymbol{N} = \begin{bmatrix} 1 & i\omega\bar{\rho}A_2L_3/A_3 \\ 0 & A_2/A_1 \end{bmatrix} \tag{70}$$

For more realistic conditions, $\boldsymbol{N}$ can be investigated through carefully chosen experiments. Typically such experiments involve introducing an acoustic source at an upstream location S in Fig. 11. The source could be an in-line siren or wall-mounted loudspeakers. By the driving of the source at a range of frequencies, $\hat{p}_1(\omega)$, $\hat{u}_1(\omega)$, $\hat{p}_2(\omega)$, and $\hat{u}_2(\omega)$ can be measured. However, the impedance $Z_2(\omega) = \hat{p}_2/\hat{u}_2$ is specified by the downstream geometry and so, for a particular downstream geometry, only the product of $\boldsymbol{N}[Z_2, 1]^T$ can be investigated. Measurements are needed with two different downstream impedances if all four coefficients are to be found. In practice, this can be done by making measurements with two different downstream lengths, or alternatively, a single length with two different exit conditions, for example, open and constricted. The advantage of this approach is that it does not rely on any modeling, assuming only that the perturbations are linear. Therefore, it gives an accurate representation of the jump or joining conditions across any geometry of premix ducts and combustion zone. Its disadvantages are that it provides little physical insight, and also measurements must be made with the flow between x_1 and x_2 representative of full-scale conditions, not only in terms of geometry, but also with the correct inlet temperature, pressure, mass flow rate, and rate of combustion. This method has been used successfully by Paschereit et al.[30] to characterize the pressure/velocity relationship across a premix duct and combustion zone in a geometry similar to that shown in Fig. 11.

An alternative approach is based on conservation equations.[33–36] The premixer geometry may be modeled by several compact area changes connected by straight ducts. At an area increase, the mass and energy fluxes are unchanged, and momentum flux increased by the axial force on the walls; hence, we may take

$$A_2\rho_2u_2 = A_1\rho_1u_1 \tag{71a}$$

$$H_2 = H_1 \tag{71b}$$

$$A_2p_2 + A_2\rho_2u_2^2 = A_2p_1 + A_1\rho_1u_1^2 \tag{71c}$$

where subscripts 1 and 2 denote the flow parameters and areas before and after the area change, respectively. (Here the pressure on the abrupt expansion has been taken to be p_1; however, some pressure recovery could be included through the use of a loss coefficient.) To find the perturbations after the area increase, Eq. (71) is linearized in the usual way to give a transfer matrix relating the downstream and upstream flow.

Table 1 Geometry and flow conditions for simple combustor (based on an atmospheric test rig)

Description	Value
Choked inlet, mass flow rate	0.05 kgs^{-1}
Choked inlet, temperature	300 K
Plenum, cross-sectional area	0.0129 m^2
Plenum, length	1.7 m
Premixer, cross-sectional area	0.00142 m^2
Fuel injection point, fuel convection time	0.006 s
Premixer, length	0.0345 m
Combustor, cross-sectional area	0.00385 m^2
Flame zone, temperature after combustion	2,000 K
Combustor, length	1.0 m
Open outlet, pressure	101,000 Pa

An area decrease can be assumed to be isentropic. This together with conversation of mass and energy gives

$$A_2\rho_2 u_2 = A_1\rho_1 u_1 \tag{72a}$$

$$H_2 = H_1 \tag{72b}$$

$$p_2/\rho_2^{\gamma} = p_1/\rho_1^{\gamma} \tag{72c}$$

For no mean flow, the jump conditions at any area change simplify to

$$[p]_1^2 = [Au]_1^2 = 0 \tag{73}$$

The flame is also treated as compact, and so Eq. (10) applies across it. However this approach needs a flame model relating the instantaneous rate of heat release to the oncoming flow. Flame models are discussed by Lieuwen,[4] but here we note that they can be determined either by analytical descriptions of the flame dynamics[9,37] or through numerical[34] or experimental investigations[38–40] of the unsteady combustion response to inlet flow disturbances. Measurements carried out at low and high pressure have remarkably similar forms[40] but different amplitudes, supporting the idea that the flame transfer function can be investigated by suitably scaled experiments or through local computational fluid dynamics solutions.

Linear Waves in the Combustor

Once the fluxes of mass, momentum, and energy are known in the combustor just downstream of the zone of combustion, the strengths of the linear waves can be calculated. Equations (7c), (7d), and (9) describe how those wave develop along the combustor, thus, determining the flow at exit. For a general value of frequency ω, this will not satisfy the downstream boundary condition. The resonant frequencies are the values of ω at which the downstream boundary condition is satisfied.

Example 5. We now consider an example of a complete system, consisting of a plenum, premix system, and combustor, similar to that shown in Fig. 11 except that the combustor has an open end. Details of the geometry are given in Table 1. A simple flame model,

$$\hat{Q}/\bar{Q} = -k(\hat{m}_i/\bar{m}_i)\exp(-i\omega\tau) \tag{74}$$

is used at the start of the combustor, where m_i is the air mass flow at the fuel injection point (taken to be at the start of premixer). The circles in Fig. 13 denote the resonant modes of the geometry for $k = 0$. Several modes are seen, all of which are stable as we would expect because there is no unsteady heat release. The premix duct provides sufficient blockage that it acts approximately like a hard end ($u' = 0$, maximum pressure amplitude) to disturbances in the plenum. This means that there is a family of resonant frequencies consisting of resonances of the plenum. In Fig. 13, these are seen at 110, 203, 289, 416, and 511 Hz, the first being the fundamental half-wave mode and the others being its harmonics. The mode at 337 Hz is the first of a family of combustor modes. Taking the front face of the combustor to be a close end gives only a very crude approximation because the discrepancy in area between combustor and premixer

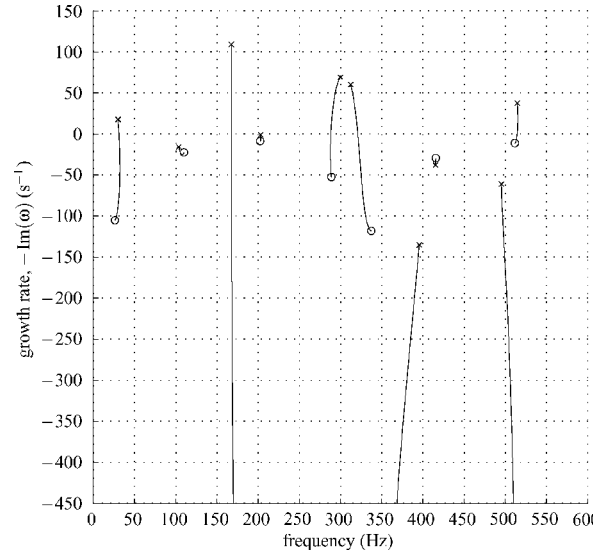

Fig. 13 Resonant modes of simple combustor: ×, modes for $k = 1$; ♀, $k = 0$, that is, no unsteady heat release; and ——, variation between these two values.

is not as large as for the plenum. The mode is somewhere between a quarter-wave and a half-wave resonance of the combustor. (Its modeshape is very similar to that in Fig. 14f.) The low-frequency mode at 30 Hz is a resonance of the geometry as a whole, specifically a quarter-wave.

We now introduce unsteady heat release by setting k to be unity. The resulting modes are denoted by crosses in Fig. 13. (The lines show the variation for k between 0 and 1.) The unsteady heat release has little effect on some modes, but generally the growth rates are increased, pushing the modes into instability. In additional to the original modes, there is a new set of modes associated with flame model. These are closely related to the additional modes for nonzero τ found in example 1: Their frequencies are approximately $1/\tau$, $2/\tau$, and $3/\tau$, and their growth rates become large and negative as k tends to zero. The modeshapes for $k = 1$ are shown in Fig. 14.

Annular Combustors

We now consider an annular gas turbine for which the plenum and combustor have a narrow annular gap cross section, as discussed earlier. Hence, we take the perturbations have the form of a circumferential mode. Wave propagation in the plenum and combustor is given by Eqs. (7c), (7d), and (9) as before. (See also the section on modal solutions.) When joining annular ducts of different inner and outer radii, considering conservation laws in a thin sector of the transition leads to the same flux relationships as for plane waves, with the addition that the angular-momentum flux is unchanged.[10] Hence, if the premix region also had an annular geometry, the perturbations for a circumferential mode can be found in much the same way as described for plane waves. Typically, however, the premix region consists of a large number of identical premix ducts evenly distributed around the circumference. Hence, there is a loss of axisymmetry, and we might expect that this would interact with the circumferential wave in the plenum to produce circumferential waves of other orders, that is, modal coupling would occur. In fact any additional modes will be high order. (See the following section on modal coupling.) Thus, it is valid to consider a single circumferential wave of a selected order in the plenum. The premix ducts will usually also be annular; however, they will have a much smaller cross section than the plenum and combustor and so, for frequencies of interest, the perturbations in them will be one dimensional. The circumferential wave in the plenum produces identical perturbations in the ducts, except that each is phase shifted. The equations relating the perturbations in the plenum to those in the premix ducts are similar to those for a simple area decrease, with adjustments due to the change from

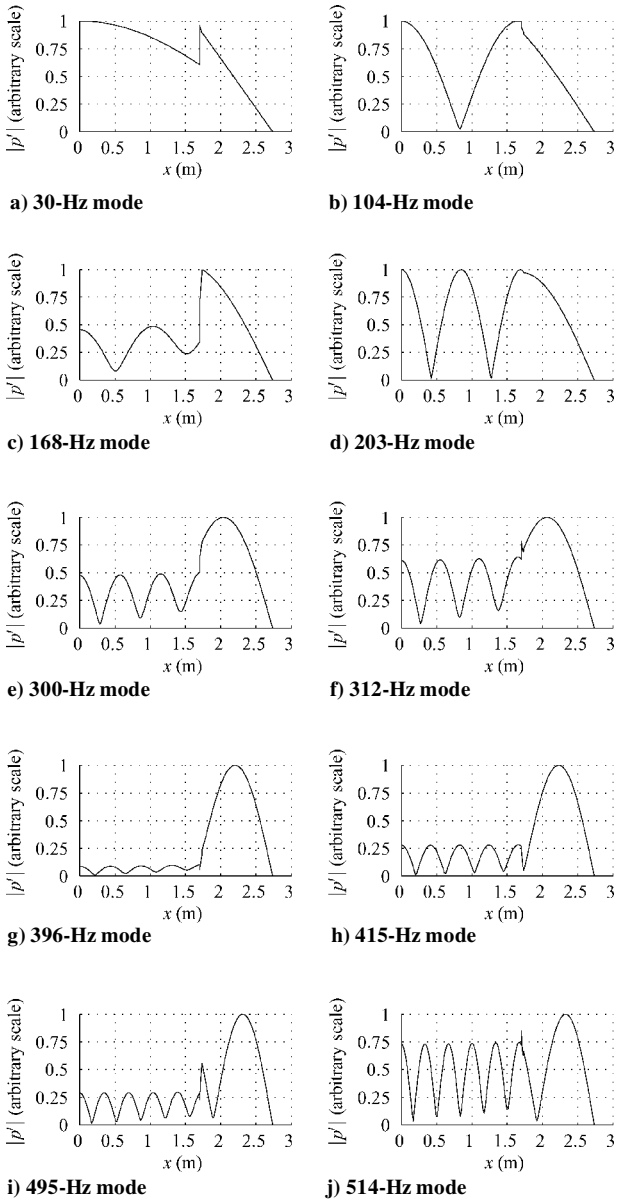

Fig. 14 Modeshapes for simple combustor, $k = 1$.

a circumferential disturbance to a set of one-dimensional perturbations. The propagation of these one-dimensional disturbances along the premix ducts can be found as before. At the inlet to the combustor, the ring of phase-shifted one-dimensional disturbances creates a circumferential wave of identical order to that in the plenum. The resonant modes for circumferential waves of this selected order can then be found by investigating the propagation of this circumferential mode through the combustor and determining the resonant frequencies at which the downstream boundary condition is satisfied.

Modal Coupling

In uniform cylindrical and annular ducts, the solutions in Eq. (59) for different values of n and m are independent and can be considered separately. However, nonuniformities can lead to a coupling of these modes. For instance, if the duct has an area change, but remains axisymmetric, the circumferential modes, that is, different values of n, are still independent but the radial modes, that is, different values of m, become coupled. Consider, for example, a circular duct that has an abrupt area increase at $x = 0$. We denote conditions in $x < 0$ by superscript (1) and in $x > 0$ by superscript (2). The duct is then $r \le b^{(1)}$ for $x < 0$ and $r \le b^{(2)}$ for $x > 0$, with $b^{(2)} > b^{(1)}$. For the case of no mean flow, only acoustic waves are present, and so from

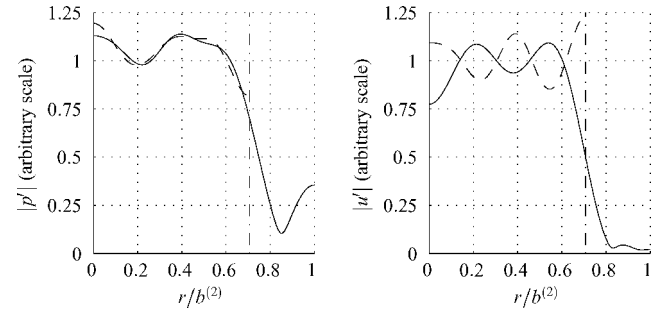

Fig. 15 Radial variation for $n = 0$ and $M = 5$: ——, $x = 0_+$; – – –, $x = 0_-$; –·–, $r = b^{(1)}$.

Eq. (59) for a given n we may write for $x < 0$

$$p' = \exp(i\omega t + in\theta) \sum_{m=1}^{\infty} \left[A_{n,m}^{+(1)} \exp(ik_{n,m}^{+} x) + A_{n,m}^{-(1)} \exp(ik_{n,m}^{-} x) \right] B_{n,m}(r) \tag{75a}$$

and for $x > 0$

$$p' = \exp(i\omega t + in\theta) \sum_{m=1}^{\infty} \left[A_{n,m}^{+(2)} \exp(ik_{n,m}^{+} x) + A_{n,m}^{-(2)} \exp(ik_{n,m}^{-} x) \right] B_{n,m}(r) \tag{75b}$$

with similar expressions for the other flow variables. Miles[41] and Alfredson[42] considered this problem for plane waves; however, the extension to $n \neq 0$ is straightforward (as is the extension to annular ducts). At $x = 0$, we must have continuity of p' and u' for $0 \le r \le b^{(1)}$ (continuity of ρ', v', and w' follow from continuity of p'), and on the rigid wall $b^{(1)} \le r \le b^{(2)}$, we require $u' = 0$. This leads to a linear system of equations relating $A_{n,m}^{\pm(1)}$ and $A_{n,m}^{\pm(2)}$. The amplitudes for one value of m are found to depend on those for all other values of m, meaning that the radial modes are coupled. In Eq. (75) we included all of the radial modes; however in practice for m sufficiently large the waves will be highly cutoff and so can be ignored. Hence, we can approximate using a finite number of radial modes, for example, $0 < m < M$. Some example results for $n = 0$ modes in a duct in which the area doubles are shown in Fig. 15. The radial variations of the magnitudes of the pressure and axial velocity on either side of the area change are shown, the solid and dashed lines denoting the values in the larger and smaller area regions, respectively. These results are for $M = 5$; as more radial modes are included, the matching becomes better and the solutions more accurate.

A similar approach was used by Akamatsu and Dowling[43] to consider three-dimensional combustion instabilities in a cylindrical combustor with a ring of premix ducts. Oscillations in the premix ducts were assumed to be one dimensional, and these were treated as point sources when joining to the combustion chamber. The loss of radial symmetry here lead to a coupling of the radial modes in the combustor. Perhaps surprisingly, because the premixers were identical and evenly distributed circumferentially, the circumferential modes remained uncoupled. Similarly, Evesque and Polifke[44] found that circumferential modes became coupled only when their premix ducts were nonidentical. In fact, it can be shown that a ring of identical premix ducts does not introduce coupling of circumferential modes provided that N is less than half the number of ducts. In other words, any coupling occurs in high-order modes that decay rapidly with axial distance and are not of practical interest.

Coupling of circumferential modes in a narrow annular gap has been considered by Stow and Dowling.[45] The presence of Helmholtz resonators in the geometry destroys the axisymmetry causing modal coupling. We now describe their method of solution because the approach should be generally applicable to finding

linear resonances in problems with modal coupling. We write $p'(t, x, \theta) = \hat{p}(x, \theta)\exp(i\omega t)$ with

$$\hat{p}(x, \theta) = \sum_{n=-\infty}^{\infty} \hat{p}_n(x)\exp(in\theta)$$

and similarly for the other variables. For $|n|$ large (for example, $|n| > N$), the mode will be highly cutoff; hence, in a similar way to the radial modes earlier, we approximate by taking

$$\hat{p}(x, \theta) = \sum_{n=-N}^{N} \hat{p}_n(x)\exp(in\theta)$$

At the inlet of the geometry, there are boundary conditions that apply to each mode independently. These define the perturbations for each circumferential mode n except for an unknown parameter λ_n. For instance, if it is an open end, $\hat{p} = 0$ for all θ, implying that $\hat{p}_n = 0$ for all n and so we may set $A_n^+ = -A_n^- = \lambda_n$ (with no entropy or vorticity waves). Here $\boldsymbol{\lambda} = [\lambda_{-N}, \ldots, \lambda_N]^T$ describes the relative amplitude and phase of the modes at the inlet and must be found as part of the solution. Similarly, at the outlet, there is a boundary condition that applies to each mode independently. We define μ_n to be the error in this boundary condition for circumferential mode n, for example, for an open end we may take $\mu_n = \hat{p}_n$. Given ω and $\boldsymbol{\lambda}$, all the circumferential components at the inlet are known. We can step through the geometry calculating all of the circumferential modes at each section before continuing to the next. For the solution thus found, each mode will have an error at the outlet, μ_n. We must find ω and $\boldsymbol{\lambda}$ to satisfying $\mu_n = 0$, thus, giving a resonance of the geometry. For a given ω, we define the matrix $\boldsymbol{M}$ to be such that $M_{n,m}$ is the value of μ_n for the solution with $\lambda_i = \delta_{i,m}$. For a general $\boldsymbol{\lambda}$, $\mu_n = M_{n,m}\lambda_m$ because the perturbations are linear. Hence, for the correct values of ω and $\boldsymbol{\lambda}$, $\boldsymbol{M\lambda} = \boldsymbol{0}$. For a solution to exist, $\boldsymbol{\lambda} \neq \boldsymbol{0}$, and so this implies that $\det \boldsymbol{M} = 0$. Thus, the procedure to find a complex resonant frequency ω is to first guess the value of ω and calculate the matrix $\boldsymbol{M}$ and then iterate the value of ω to achieve $\det \boldsymbol{M} = 0$. For this value of ω, a $\boldsymbol{\lambda}$ will exist giving $\boldsymbol{M\lambda} = \boldsymbol{0}$. Finally, this correct $\boldsymbol{\lambda}$ is calculated using an inverse iteration method ($\boldsymbol{M\lambda}_{\text{new}} = \boldsymbol{\lambda}_{\text{old}}$). The modeshape for the resonance can then be calculated using this $\boldsymbol{\lambda}$. As before, the resonant frequency and growth rate are given by ω.

Conclusions

A series of model problems with very simple geometries has been considered to investigate the modal analysis of the various components that make up a gas turbine combustion system.

The form of the coupling between the heat input and the unsteady flow has been demonstrated to have a crucial effect on the frequency of oscillation. A one-term Galerkin series expansion is not adequate to determine this frequency shift for the sorts of unsteady combustion response typical of gas turbine combustors. The effect of the mean temperature ratio across the combustion zone can be significant. Mean flow effects are not significant for Mach numbers less than about 0.2; however, a mean flow does introduce the possibility of a new mode of oscillation: one at much lower frequency where the period of oscillation is set primarily by the time taken for the convection of entropy waves, or hot spots. Higher-order modes in the annular and cylindrical ducts bring in the possibility that the modes are cutoff. We have described how a typical LPP combustion system can be built up and analyzed through connection of a series of cylindrical and/or annular ducts. In many geometries, the premixed ducts provide sufficient blockage that these modes of oscillation are close to separate modes of the plenum and combustor with a hard or approximately constant velocity boundary condition at the premixer. Finally, we have noted that modal coupling may occur when the geometry is no longer axisymmetric.

The models presented apply to small linear oscillations, not to the large-amplitude limit cycles that cause problems in gas turbines. However, linear models can provide important information to gas turbine designers and operators. First, the models give predictions of linear instability boundaries. An oscillation will always be small to begin with, and if it is linearly stable, it will not grow to form a limit cycle. Second, the frequency of a linear mode provides a good approximation to that of the resulting limit cycle. Damage is often the result of a oscillation frequency being close to a structural resonant frequency of a component of the gas turbine, and so knowledge of potential frequencies can be very useful. Finally, linear models can be adapted to give predictions of limit-cycle amplitude. The main effect determining the limit-cycle amplitude is likely to be a saturation of the heat release oscillation from the flame. One may assume that elsewhere nonlinear effects are less important, and so the linear models are still applicable except for that there is an amplitude dependence in the flame model. A describing function analysis can then be used to give predictions of limit-cycle frequencies and amplitudes instead of linear frequency and growth rate (Dowling[14]). The great advantage of the linear approaches presented is their speed. Many geometry configurations and operating conditions can be investigated in a relatively short time.

Appendix: Derivation of Equation (42)

When heat conduction and viscous effects are neglected, the entropy equation (4) simplifies to

$$\rho T\frac{\mathrm{D}S}{\mathrm{D}t} = q \tag{A1}$$

Replacing S by the perfect gas form $S = c_v \log p - c_p \log \rho$, we obtain

$$\frac{\rho T c_v}{p}\frac{\mathrm{D}p}{\mathrm{D}t} = -c_p T\frac{\mathrm{D}\rho}{\mathrm{D}t} + q \tag{A2}$$

After substitution for $\mathrm{D}\rho/\mathrm{D}t$ from the equation of mass conservation, we obtain

$$\frac{c_v}{R_{\text{gas}}}\frac{\mathrm{D}p}{\mathrm{D}t} = c_p T\rho\nabla\cdot\boldsymbol{u} + q \tag{A3}$$

which is equivalent to

$$\frac{\mathrm{D}p}{\mathrm{D}t} = c^2\rho\nabla\cdot\boldsymbol{u} + (\gamma - 1)q \tag{A4}$$

since $c^2 = \gamma R_{\text{gas}}T$ and $R_{\text{gas}}/c_v = \gamma - 1$. Equation (42) is the linearized form of Eq. (A4).

References

[1]Rayleigh, L., *The Theory of Sound*, Macmillan, London, 2nd edition, Vol. 2, 1896, pp. 224–234.

[2]Crocco, L., and Cheng, S.-I., *Theory of Combustion Instability in Liquid Propellant Rocket Motors*, Butterworths, London, 1956.

[3]Kuo, K. K., and Summerfield, M. (eds.), *Fundamentals of Solid-Propellant Combustion*, Progress in Astronautics and Aeronautics, Vol. 90, AIAA, New York, 1984.

[4]Lieuwen, T., "Modeling Premixed Combustion–Acoustic Wave Interations: A Review," *Journal of Propulsion and Power*, Vol. 19, No. 5, 2003, pp. 765–781.

[5]Keller, J. J., "Thermoacoustic Oscillations in Combustion Chambers of Gas Turbines," *AIAA Journal*, Vol. 33, No. 12, 1995, pp. 2280–2287.

[6]Hsiao, G. C., Pandalai, R. P., Hura, H. S., and Mongia, H. C., "Combustion Dynamic Modeling for Gas Turbine Engines," AIAA Paper 98-3380, July 1998.

[7]Hsiao, G. C., Pandalai, R. P., Hura, H. S., and Mongia, H. C., "Investigation of Combustion Dynamics in Dry-Low-Emission (DLE) Gas Turbine Engines," AIAA Paper 98-3381, July 1998.

[8]Lovett, J. A., Chu, W.-W., and Shah, S. N., "Modeling of Combustion Chamber Acoustics and Control of Combustion Instabilities in Gas Turbines," *6th International Congress on Sound and Vibration*, July 1999.

[9]Dowling, A. P., and Hubbard, S., "Instability in Lean Premixed Combustors," *Journal of Power and Energy*, Vol. 214, No. A4, 2000, pp. 317–332.

[10]Stow, S. R., and Dowling, A. P., "Thermoacoustic Oscillations in an Annular Combustor," American Society of Mechanical Engineers, ASME Paper 2001-GT-0037, June 2001.

[11]Chu, B.-T., and Kovasznay, L. S. G., "Non-linear Interactions in a Viscous Heat-Conducting Compressible Gas," *Journal of Fluid Dynamics*, Vol. 3, No. 5, 1958, pp. 494–514.

[12]Marble, F. E., and Candel, S. M., "Acoustic Disturbance from Gas Non-uniformities Convected Through a Nozzle," *Journal of Sound and Vibration*, Vol. 55, No. 2, 1977, pp. 225–243.

[13]Stow, S. R., Dowling, A. P., and Hynes, T. P., "Reflection of Circumferential Modes in a Choked Nozzle," *Journal of Fluid Dynamics*, Vol. 467, Sept. 2002, pp. 215–239.

[14]Dowling, A. P., "A Kinematic Model of a Ducted Flame," *Journal of Fluid Dynamics*, Vol. 394, Sept. 1999, pp. 51–72.

[15]Culick, F. E. C., "Combustion Instabilities in Liquid-Fueled Propulsion Systems—An Overview," *AGARD Conference Proceedings*, No. 450, 1989, Paper 1.

[16]Dowling, A. P., "The Calculation of Thermoacoustic Oscillations," *Journal of Sound and Vibration*, Vol. 180, No. 4, 1995, pp. 557–581.

[17]Annaswamy, A. M., Fleifil, M., Hathout, J. P., and Ghoniem, A. F., "Impact of Linear Coupling on Design of Active Controllers for Thermoacoustic Instability," *Combustion Science and Technology*, Vol. 128, No. 1–6, 1997, pp. 131–160.

[18]Cummings, A., "Ducts with Axial Temperature Gradients: An Approximate Solution for Sound Transmission and Generation," *Journal of Sound and Vibration*, Vol. 51, No. 1, 1977, pp. 55–67.

[19]Jones, H., "The Mechanics of Vibrating Flames in Tubes," *Proceedings of the Royal Society of London, Series A: Mathematical and Physical Sciences*, Vol. 353, No. 1675, 1977, pp. 459–473.

[20]Sujith, R. I., Waldherr, G. A., and Zinn, B., "An Exact Solution for One-Dimensional Acoustic Fields in Ducts with an Axial Temperature Gradient," *Journal of Sound and Vibration*, Vol. 184, No. 3, 1995, pp. 389–402.

[21]Kumar, B. M., and Sujith, R. I., "Exact Solution for One-Dimensional Acoustic Fields in Ducts with Polynomial Mean Temperature Profiles, *Journal of Vibration and Acoustics*, Vol. 120, No. 4, 1998, pp. 965–969.

[22]Karthik, B., Kumar, B. M., and Sujith, R. I., "Exact Solutions to One-Dimensional Acoustic Fields with Temperature Gradient and Mean Flow, *Journal of the Acoustical Society of America*, Vol. 108, No. 1, 2000, pp. 38–43.

[23]Sujith, R. I., "Exact Solutions for Modeling Sound Propagation Through a Combustion Zone," *Journal of the Acoustical Society of America*, Vol. 110, No. 4, 2001, pp. 1839–1844.

[24]Eisenberg, N. A., and Kao, T. W., "Propagation of Sound Through a Variable Area Duct with Steady Compressible Flow," *Journal of the Acoustical Society of America*, Vol. 49, No. 1, 1971, pp. 169–175.

[25]Subrahmanyam, P. B., Sujith, R. I., and Lieuwen, T., "A Family of Exact Transient Solutions for Acoustic Wave Propagation in Inhomogeneous, Non-uniform Area Ducts," *Journal of Sound and Vibration*, Vol. 240, No. 4, 2001, pp. 705–715.

[26]Zhu, M., Dowling, A. P., and Bray, K. N. C., "Self-Excited Oscillations in Combustors with Spray Atomisers," *Journal of Engineering for Gas Turbines and Power*, Vol. 123, No. 5, 2001, pp. 779–786.

[27]Watson, G. N., *A Treatise on the Theory of Bessel Functions*, 2nd ed., Cambridge Univ. Press, Cambridge, England, U.K., 1944, p. 482.

[28]Eversman, W., "Theoretical Models for Duct Acoustic Propagation and Radiation," *Aeroacoustics of Flight Vehicles: Theory and Practice*, edited by H. H. Hubbard, Vol. 2, Acoustical Society of America, New York, 1994, Chap. 13, pp. 101–163.

[29]Tyler, J. M., and Sofrin, T. G., "Axial Compressor Noise Studies," *SAE Transactions*, Vol. 70, 1962, pp. 309–332.

[30]Paschereit, C. O., Schuermans, B., Polifke, W., and Mattson, O., "Measurement of Transfer Matrices and Source Terms of Premixed Flames," *Journal of Engineering for Gas Turbines and Power*, Vol. 124, No. 2, 2002, pp. 239–247.

[31]Ohtsuka, M., Yoshida, S., Inage, S., and Kobayashi, N., "Combustion Oscillation Analysis of Premixed Flames at Elevated Pressures," American Society of Mechanical Engineers, ASME Paper 98-GT-581, June 1998.

[32]Hobson, D. E., Fackrell, J. E., and Hewitt, G., "Combustion Instabilities in Industrial Gas Turbines—Measurements on Operating Plant and Thermoacoustic Modeling," *Journal of Engineering for Gas Turbines and Power*, Vol. 122, No. 3, 2000, pp. 420–428.

[33]Dowling, A. P., "Thermoacoustic Instability," *6th International Congress on Sound and Vibration*, July 1999.

[34]Krüger, U., Hürens, J., Hoffmann, S., Krebs, W., and Bohn, D., "Prediction of Thermoacoustic Instabilities with Focus on the Dynamic Flame Behavior for the 3A-Series Gas Turbine of Siemens KWU," American Society of Mechanical Engineers, ASME Paper 99-GT-111, June 1999.

[35]Krüger, U., Hürens, J., Hoffmann, S., Krebs, W., Flohr, P., and Bohn, D., "Prediction and Measurement of Thermoacoustic Improvements in Gas Turbines with Annular Combustion Systems," *Journal of Engineering for Gas Turbines and Power*, Vol. 123, No. 3, 2001, pp. 557–566.

[36]Lovett, J. A., and Uznanski, K. T., "Prediction of Combustion Dynamics in a Staged Premixed Combustor," American Society of Mechanical Engineers, ASME Paper GT-2002-30646, June 2002.

[37]Ni, A., Polifke, W., and Joos, F., "Ignition Delay Time Modulation as a Contribution to Thermo-acoustic Instability in Sequential Combustion," American Society of Mechanical Engineers, ASME Paper 2000-GT-0103, May 2000.

[38]Lawn, C. J., "Interaction of the Acoustic Properties of a Combustion Chamber with Those of Premixture Supply," *Journal of Sound and Vibration*, Vol. 224, No. 5, 1999, pp. 785–808.

[39]Krebs, W., Hoffmann, S., Prade, B., Lohrman, M., and Büchner, H., "Thermoacoustic Flame Responce of Swirl Flames," American Society of Mechanical Engineers, ASME Paper GT-2002-30065, June 2002.

[40]Cheung, W. S., Sims, G. J. M., Copplestone, R. W., Tilston, J. R., Wilson, C. W., Stow, S. R., and Dowling, A. P., "Measurement and Analysis of Flame Transfer Function in a Sector Combustor under High Pressure Conditions," American Society of Mechanical Engineers, ASME Paper GT2003-38219, June 2003.

[41]Miles, J., "The Reflection of Sound Due to a Change in Cross Section of a Circular Tube," *Journal of the Acoustical Society of America*, Vol. 16, No. 1, 1944, pp. 14–19.

[42]Alfredson, R. J., "The Propagation of Sound in a Circular Duct of Continuously Varying Cross-Sectional Area," *Journal of Sound and Vibration*, Vol. 23, No. 4, 1972, pp. 433–442.

[43]Akamatsu, S., and Dowling, A. P., "Three Dimensional Thermoacoustic Oscillation in an Premix Combustor," American Society of Mechanical Engineers, ASME Paper 2001-GT-0034, June 2001.

[44]Evesque, S., and Polifke, W., "Low-Order Acoustic Modelling for Annular Combustors: Validation and Inclusion of Modal Coupling," American Society of Mechanical Engineers, ASME Paper GT-2002-30064, June 2002.

[45]Stow, S. R., and Dowling, A. P., "Modelling of Circumferential Modal Coupling Due to Helmholtz Resonators," American Society of Mechanical Engineers, ASME Paper GT2003-38168, June 2003.